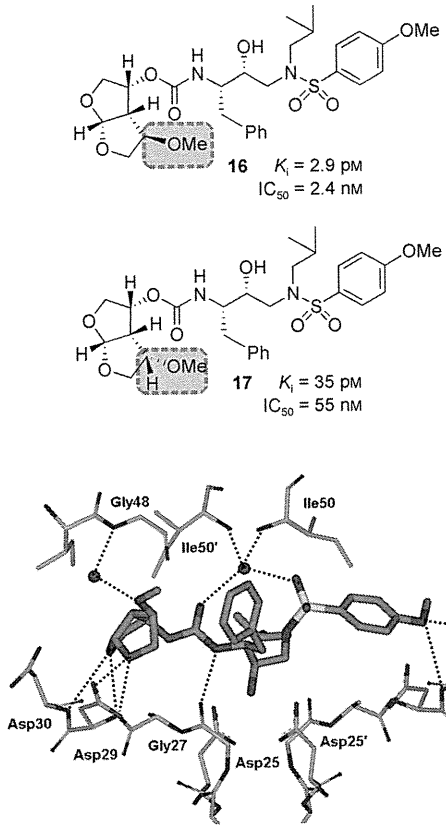

Figure 13. Structures of PIs **16** and **17** and the X-ray structure of **16**-bound HIV-1 protease.

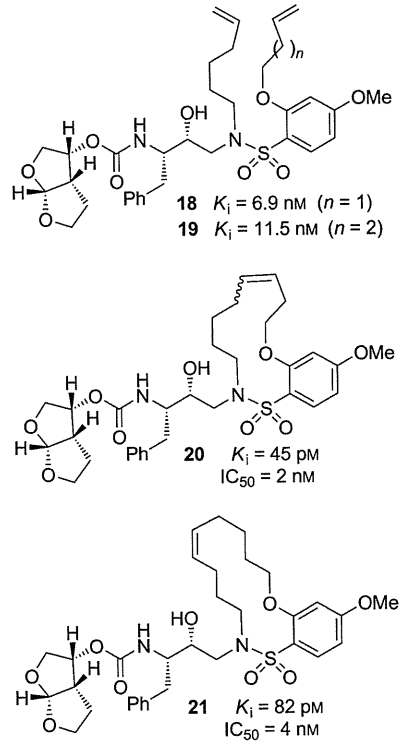

Figure 14. Structures of acyclic and macrocyclic PIs **18–21**.

subsite. The structural studies of A-77003[126] indicated that the V82A mutant results in decreased van der Waals interactions with the phenyl rings in both the S1 and S1′ subsites.[127] Also, there was evidence of the repacking of the inhibitor side chain and protease atoms in the S1 subsite. Based upon this insight, we envisioned that 11- to 15-membered saturated and unsaturated macrocycles would effectively fill the S1′–S2′ subsites. As shown in Figure 14, macrocyclic inhibitors **20** and **21** displayed excellent enzyme inhibitory and antiviral activity; however, their acyclic homologues were significantly less potent. Also, saturated inhibitors were less active than their unsaturated analogues.[95]

To ascertain if the structural effects led to improved drug-resistance properties, inhibitors **20** and **21** were evaluated against a panel of clinical wild-type X_4-HIV-1 isolates (HIV-$1_{ERS104pre}$) along with various multidrug-resistant clinical X_4- and R_5-HIV-1 isolates using PBMCs as target cells.[95,105] As shown in Table 8, the potency of both inhibitors against HIV-$1_{ERS104pre}$ (IC_{50} = 7 and 5 nM, respectively) was superior to that of the approved inhibitors IDV, APV, and LPV but nearly twofold less potent than darunavir (IC_{50} = 3 nM).[95] Inhibitor **20** showed better potency than amprenavir against HIV-$1M_{DR/C}$, HIV-$1M_{DR/G}$, HIV-$1M_{DR/TM}$, and HIV-$1M_{DR/JSL}$ and was six times more potent against HIV-$1M_{DR/MM}$. Inhibitor **21** also displayed superior potency against HIV-$1M_{DR/C}$ and HIV-$1M_{DR/G}$ (greater than 12- and 15-fold, respectively) compared to amprenavir.[95,128] Furthermore, both macrocyclic PIs prevented the replication of HIV-1_{NL4-3} variants selected against up to 5 μM of saquinavir, lopinavir, and indinavir with IC_{50} values of 20 nM to 46 nM. We have determined an X-ray crystal structure of **20**-bound HIV-1 protease at 1.17 Å resolution. As can be seen in Figure 15, both P2 and P2′ ligands are involved in extensive hydrogen-

Table 8: Antiviral activity of macrocyclic inhibitors against multidrug-resistant clinical isolates in PHA-PBMCs.

Virus[a]	IC_{50} value [μM]						
	SQV	IDV	APV	LPV	DRV	**21**	**20**
HIV-$1_{ERS104pre}$ (WT X4)	0.008	0.043	0.030	0.034	0.003	0.007	0.005
HIV-$1_{MDR/B}$ (X4)	0.27 (34)	>1 (>23)	>1 (>33)	>1 (>29)	0.019 (6)	0.089 (13)	0.037 (7)
HIV-$1_{MDR/C}$ (X4)	0.032 (11)	>1 (>23)	0.37 (12)	>1 (>29)	0.008 (3)	0.029 (4)	0.044 (9)
HIV-$1_{MDR/G}$ (X4)	0.030 (4)	0.34 (5)	0.43 (14)	0.26 (8)	0.023 (5)	0.028 (4)	0.057 (11)
HIV-$1_{MDR/TM}$ (X4)	0.26 (33)	>1 (>23)	0.32 (11)	>1 (>29)	0.004 (1)	0.072 (10)	0.027 (6)
HIV-$1_{MDR/MM}$ (R5)	0.19 (24)	>1 (>23)	0.21 (7)	>1 (>29)	0.011 (4)	0.055 (8)	0.033 (7)
HIV-$1_{MDR/JSL}$ (R5)	0.30 (37)	>1 (>23)	0.62 (21)	>1 (>29)	0.027 (9)	0.21 (30)	0.073 (15)

[a] The amino acid substitutions identified in the protease-encoding region compared to the consensus type B sequence cited from the Los Alamos database. See reference [95] for details.

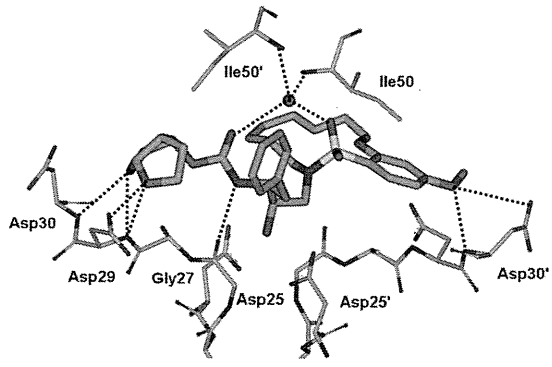

Figure 15. X-ray structure of HIV-1 protease bound to the macrocyclic inhibitor **20**. All strong hydrogen-bonding interactions are shown as dotted lines.

bonding interactions with the protein backbone atoms in both the S2 and S2′ subsites, similar to inhibitor **10**. The crown-shaped P1′–P2′macrocycle nicely fills the S1′ pocket. Interestingly, the macrocycle acts more or less like a spring and pushes against the P1 phenyl ring. This causes a rotation about 30° towards Asp29′ along the backbone which is absent in the X-ray structure of **10**-bound HIV-1 protease. Both macrocyclic PIs were able to maintain excellent potency against multidrug-resistant clinical isolates possibly because of their ability to make extensive hydrogen bonds with the protease backbone as well as their hydrophobic interactions in the S1′–S2′ subsites.[95]

6. Probing the Backbone-Binding Concept as a Design Strategy to Combat Drug Resistance

6.1. Development of Cyclopentanyltetrahydrofuran (Cp-THF) as a Novel P2 Ligand

To further investigate the merit of targeting the protein backbone as a design strategy, based upon various protein–ligand X-ray structures, we decided to design structurally different cyclic-ether-derived ligands that were not related to bis-THF ligand. This effort led to the design of a stereochemically defined bicyclic hexahydrocyclopentanofuran (Cp-THF) as the P2 ligand. Incorporation of this ligand in the hydroxyethylaminosulfonamide isostere provided a series of exceptionally potent PIs.[51] We positioned the cyclic ether oxygen in the Cp-THF ring to form hydrogen bonds with the backbone NH groups of Asp29 and Asp30. As can be seen in Figure 16, replacing the bis-THF in darunavir with a new Cp-THF ligand provided inhibitor **22**, which exhibited subnanomolar enzyme inhibitory potency nearly ten times less than that of darunavir ($K_i = 16$ pM). We believed that binding of the Cp-THF ligand in the S2 subsite was distinct from the bis-THF ligand and may have caused a slight shift in position of the remainder of the inhibitor structure within the active site.[51] We then speculated that modifications of the P2′ aniline could allow improved interactions with the NH groups of Asp29′ and Asp30′ in the S2′ subsite. As shown, we have incorporated a hydroxymethylsulfonamide as the P2′ ligand

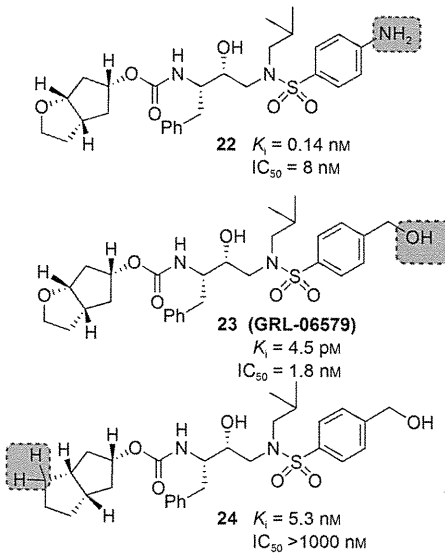

Figure 16. Structures of Cp-THF-related PIs.

and the resulting inhibitor **23** showed a 30-fold improvement of enzyme inhibition ($K_i = 4.5$ pM) compared to **22**. In addition, it has shown very impressive antiviral potency ($IC_{50} = 1.8$ nM) similar to that of inhibitor **10**. In order to probe the importance of the Cp-THF ring oxygen, we synthesized inhibitor **24** in which the oxygen is replaced with a methylene group. Interestingly, **24** displayed a more than 1100-fold loss of enzyme inhibitory potency compared to **23**. Furthermore, **24** exhibited a drastic loss in antiviral activity ($IC_{50} > 1000$ nM). This result indicated that the Cp-THF ring oxygen is involved in critical interactions in the active site.

We determined the X-ray crystal structure of **23**-bound HIV-1 protease at a 1.35 Å resolution and this high-resolution structure provided critical molecular insight into the interactions at the ligand binding site.[51] As shown in Figure 17, inhibitor **23** makes extensive interactions in the active site similar to darunavir. The P2′ hydroxy group forms a strong hydrogen bond to the backbone NH group of Asp30′and a water-mediated contact with the side chain oxygen of Asp30′. The ring oxygen of the P2 Cp-THF ligand forms a strong hydrogen bond with the backbone NH group of Asp29 and a weak hydrogen bond with Asp30. These interactions cannot

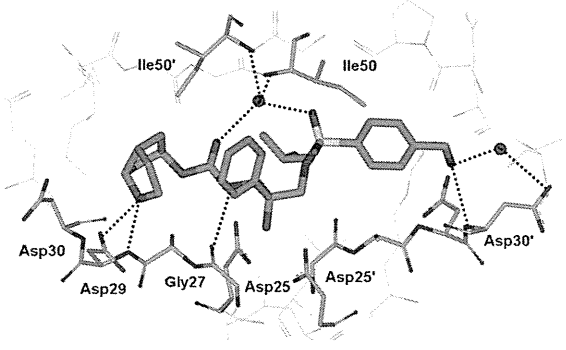

Figure 17. X-ray structure of **23**-bound HIV-1 protease.

occur for inhibitor **24** which lacks the ring oxygen and this may explain why **24** is significantly less potent than **23**. This result illustrates the importance of forming hydrogen bonds with the protease backbone in the S2 subsite and suggests that simply filling the binding space of this site is not sufficient to induce tight binding and elicit a biological response.

We superimposed the X-ray structure of **23**-bound HIV-1 protease (wild-type) with the three most highly mutated drug-resistant proteases.[51] These structures showed minimal root-mean-square deviation of the α-carbon backbone atoms (0.5 to 1.1 Å) suggesting inhibitor **23** should retain good to excellent contacts with the backbone of the mutant proteases. As it turned out, inhibitor **23** exerted very potent activity against HIV-1 isolates (HIV-1_{LAI} and HIV-$1_{Ba\text{-}L}$) in both MT-2 cells and PHA-PBMC (Table 10). Furthermore, as evident in Table 9, inhibitor **23** retained significant antiviral activity against a panel of HIV-1 drug-resistant viral strains. Inhibitor **23** displayed the most potent activity ($IC_{50}=3$ nM) against HIV-1 clinical strain HIV-1_{ET}, which had been isolated from a drug-naive patient. Furthermore, six drug-resistant clinical strains containing 10–12 amino acid substitutions associated with protease inhibitor resistance (HIV-1_B, HIV-1_C, HIV-1_G, HIV-1_{TM}, HIV-1_{EV}, and HIV-1_{ES}) were isolated from patients with HIV-1 infection having received 7–11 different antiviral agents for 24 to 81 months.[82,105] All tested approved PIs were highly resistant. However, inhibitor **23** exerted highly potent activity against all of these six variants with IC_{50} values ranging from 4 nM to 52 nM. Inhibitor **23** was also highly potent against HIV-1_K with an IC_{50} value as low as 3 nM. This data indicate that inhibitor **23** is highly active against a wide spectrum of drug-resistant variants.[51]

Table 10: Antiviral activity (IC_{50}) of **23** in PBMC and MT-2 cells.

Virus	IC_{50} [nM][a]					
	SQV	RTV	INV	NFV	APV	**23**
HIV-1_{LAI}	14	43	32	14	34	1.8
HIV-$1_{Ba\text{-}L}$	18	36	24	7	29	2.0
HIV-1_{LAI}	24	34	26	10	24	1.8
HIV-2_{EHO}	1.9	290	13	20	440	21

[a] Data represent the mean value of three determinations. See reference [51] for details.

6.2. Design of meso-Hexahydrocyclopenta-1,3-dioxolane as a P2 Ligand

As we have seen, the oxygen atom in the Cp-THF ring of **23** is critical to its superb antiviral and anti-drug-resistance properties. Based upon the X-ray structure of **23**-bound HIV-1 protease, we then speculated that a corresponding *meso*-hexahydrocyclopenta-1,3-dioxolane ligand would be able to maintain interactions similar to those of the Cp-THF ligand. Essentially, we would insert an oxygen atom into the Cp-THF ring and form a *meso*-hexahydrocyclopenta-1,3-dioxolane ligand which would greatly reduce the stereochemical complexity and allow for a simplified synthetic pathway. In addition to the synthetic advantage, we postulated that the additional ether oxygen may engage in hydrogen-bonding interactions with the protease thereby enhancing the potency of the PIs. Figure 18 depicts the structure and potency of a number of PIs incorporating a *meso* ligand.[129]

The *syn* isomer **25** demonstrated enzyme inhibitory potency and antiviral activity comparable to that of the Cp-THF-derived PI **23**, whereas the *anti* isomer **27** showed a threefold decrease in potency. Unlike the results with the Cp-THF ligand, incorporation of a hydroxymethyl group in the P2′ ligand resulted in a slight reduction in potency. We next explored a 1,4-dioxane P2 ligand; the resulting inhibitor **28** exhibited a significant reduction in antiviral potency. A larger trioxepane system also provided a less active PI. We evaluated **25** against a panel of multidrug-resistant HIV-1 variants, and the results are shown in Table 11. Inhibitor **25** exhibited antiviral activity comparable to that of the approved PIs SQV and APV, while it outperformed IDV. However, **25** was not as active as darunavir against the wild-type or drug-resistant HIV-1 clinical variants. We determined an X-ray structure of **28**-bound HIV-1 protease at 1.07 Å resolution (Figure 19). The inhibitor binds with extensive interactions in the protease active site. Interestingly, one of the dioxane oxygens forms a hydrogen bond with the backbone NH group of Asp29. The other oxygen is involved in a water-mediated hydrogen bond with the amide NH group of Gly48. These interactions with Gly48 were similar to those reported for several peptide substrate analogues.[15,64] How-

Table 9: Antiviral activity of **23** against a panel of HIV-1 viral strains.

Virus	IC_{50} [nM] values						
	SQV	RTV	IDV	NFV	APV	DRV	**23**
HIV-1_{ET}	17	15	30	32	23	n.d.	3
HIV-1_B	230	>1000	>1000	>1000	290	10.2	15
HIV-1_C	100	>1000	500	310	300	3.5	5
HIV-1_G	59	>1000	500	170	310	3.7	20
HIV-1_{TM}	250	>1000	>1000	>1000	220	3.5	4
HIV-1_{EV}	>1000	>1000	>1000	>1000	>1000	n.d.	52
HIV-1_{ES}	>1000	>1000	>1000	>1000	>1000	n.d.	31
HIV-1_K	20	58	260	>1000	68	3	3

[a] Amino acid substitutions identified in the protease-encoding region of HIV-1_B (B), HIV-1_C (C), HIV-1_G (G), HIV-1_{TM} (TM), HIV-1_{EV} (EV), HIV-1_{ES} (ES), HIV-1_{ET} (ET), HIV-1_K (NFV_R) as compared to the consensus B sequence cited from the Los Alamos data base. All values were determined in triplicate. The IC_{50} values were determined by employing PHA-PBMC as target cells and the inhibition of p24 Gag protein production as the endpoint. See reference reference [51] for details.

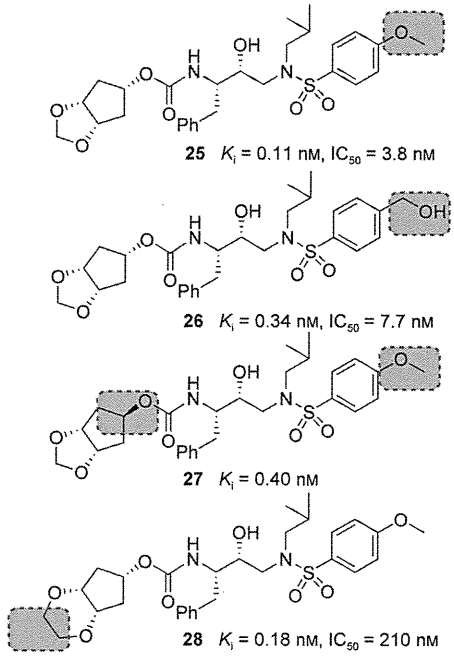

Figure 18. Enzyme K_i values and antiviral potency of PIs **25–28**.

ever, this interaction with Gly48 has not been previously utilized in ligand design. Based upon this X-ray structure, we created an active model of **25**. It appears that smaller the 1,3-dioxolane forms an additional hydrogen bond with the backbone NH group of Asp30.[129] This additional hydrogen bond may explain the increased antiviral activity of **25** relative to **28**.

6.3. Alkoxy/Hydroxy-Cp-THF Ligands and Their Effect on Drug-Resistance Properties

As described above, the *meso*-dioxolane-derived inhibitor exhibited very potent enzyme inhibitory and antiviral activity.[129] As shown in Figure 19, we speculated that both oxygens of the dioxolane ring in **25** form hydrogen bonds with backbone Asp29 and Asp30 NH groups and also form a water-mediated hydrogen bond with the Gly48 backbone NH group. Based upon these possible interactions in the ligand binding site, we subsequently designed a 3-hydroxy-Cp-THF derivative to interact with the Gly48 NH group in the flap.[130] We synthesized a stereochemically defined alkoxy-Cp-THF

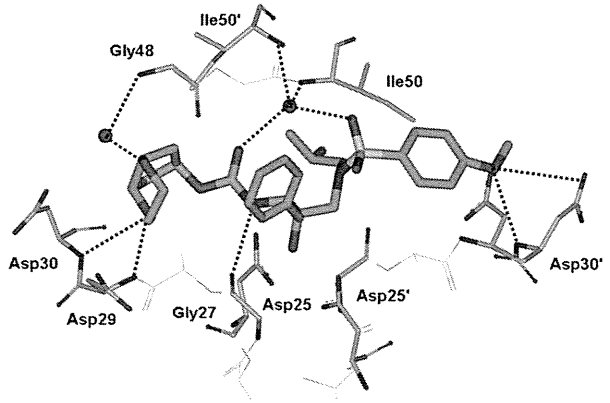

Figure 19. X-ray structure of inhibitor **28** bound to the active site of wild-type HIV-1 protease.

derivative and converted it into the PIs shown in Figure 20. As can be seen, inhibitor **30** with a 3*R*-hydroxy group showed the most potent antiviral activity comparable to that of

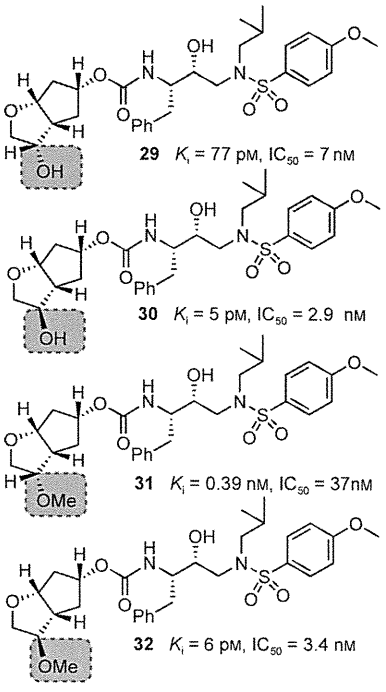

Figure 20. Structures of PIs **29–32** with alkoxy/hydroxy-Cp-THF ligands.

Table 11: Antiviral activity of inhibitor **25** against clinical HIV-1 isolates in PBMC cells.

Virus[a]	IC_{50} values [nM]				
	SQV	IDV	APV	DRV	**25**
$HIV\text{-}1_{ERS104pre}$ (wild-type: X4)	12	26	33	3.5	29
$HIV\text{-}1_{MDR/MM}$ (R5)	190 (16)	>1000 (>38)	300 (9)	17 (5)	150 (5)
$HIV\text{-}1_{MDR/JSL}$ (R5)	330 (28)	>1000 (>38)	430 (13)	26 (7)	550 (19)
$HIV\text{-}1_{MDR/C}$ (X4)	36 (3)	>1000 (>38)	230 (7)	7 (2)	300 (10)
$HIV\text{-}1_{MDR/G}$ (X4)	29 (2)	290 (11)	340 (10)	7 (2)	340 (12)
$HIV\text{-}1_{MDR/A}$ (X4)	81 (7)	>1000 (>38)	100 (3)	3 (1)	21 (1)

[a] Amino acid substitutions identified in the protease-encoding region compared to the consensus type B sequence cited from the Los Alamos database, see reference [129] for details.

darunavir. The related inhibitor **29** with a 3*S*-hydroxy group was also quite potent. We prepared the corresponding 3-methoxy-Cp-THF ligands and the resulting inhibitors **31** and **32** showed stereochemical preferences and potencies similar to those of the corresponding hydroxy derivatives.[130]

We then determined the X-ray crystal structure of **30**-bound HIV-1 protease at 1.23 Å resolution. As shown in Figure 21, the Cp-THF ring oxygen forms a strong hydrogen bond with the Asp29 NH group and a rather weak hydrogen bond with the Asp29 carboxylate. The 3-hydroxy group appears to form a nice water-mediated hydrogen bond with the Gly48 backbone NH group.

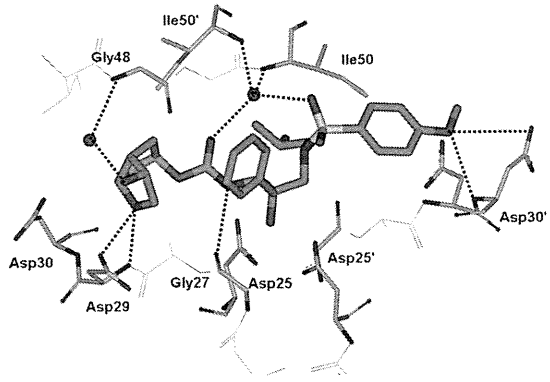

Figure 21. X-ray structure of **30**-bound HIV-1 protease.

PIs **29** and **30** were evaluated against a panel of multidrug-resistant HIV-1 variants and compared with the approved PIs darunavir and APV (Table 12). The activity of inhibitor **30** against various multidrug-resistant HIV-1 variants is similar

Table 12: Comparison of the antiviral activity of **29**, **30**, and of other PIs against multidrug-resistant HIV-1 variants.

Virus[a]	IC_{50} [μM] (fold change)			
	APV	DRV	**29**	**30**
$HIV\text{-}1_{ERS104pre}$ (wild type)	0.030	0.0037	0.020	0.0029
$HIV\text{-}1_{MDR/B}$	0.93 (31)	0.036 (10)	>1 (>50)	0.029 (10)
$HIV\text{-}1_{MDR/C}$	0.26 (9)	0.013 (4)	>1 (>50)	0.022 (7)
$HIV\text{-}1_{MDR/G}$	0.38 (12)	0.0023 (1)	0.27 (13)	0.0045 (2)
$HIV\text{-}1_{MDR/TM}$	0.19 (6)	0.0019 (1)	0.041 (2)	0.0031 (1)

[a] Amino acid substitutions identified in the protease-encoding region compared to the consensus type B sequence cited from the Los Alamos database, see reference [130] for details.

to that of darunavir.[130] The changes in the IC_{50} values with **30** were similar to those with darunavir. In contrast, PI **29** with a 3*S*-hydroxy ligand lost potency significantly. Also, APV showed high IC_{50} values and lower resilience against the drug-resistant HIV-1 strains examined. The X-ray structure of **30**-bound HIV-1 protease and its resistance profile further supported the backbone-binding strategy for combating drug resistance.

6.4. Further Enhancing the Backbone Interactions of Cp-THF-Derived PIs at the S1′ Site and Probing the Effect on Drug-Resistance Properties

In addition to ligand design to enhance interactions with the protein backbone in the S2 subsite, we have also expanded our design concept in other regions of the protease active site. We particularly planned to design PIs with new P1′ ligands in place of the isobutyl group of **23** that could interact with backbone atoms as well as fill the hydrophobic pocket in S1′ subsite. We explored the incorporation of stereochemically defined 2-pyrrolidinone and oxazolidinone functionalities so that the pyrrolidinone NH group could form a hydrogen bond with Gly27′ and its carbonyl group could interact with Arg8′ in the S1′ site.[131] Our initial plan was to examine the potential of the new P1′ ligand in combination with Cp-THF and bis-THF ligands. We also wanted to address the question of whether enhancement of backbone-binding interactions would lead to PIs with improved drug-resistance profiles. The results of this investigation are summarized in Figure 22. Inhibitor **33** with (*S*)-methyl-2-pyrrolidinone as the P1′ ligand

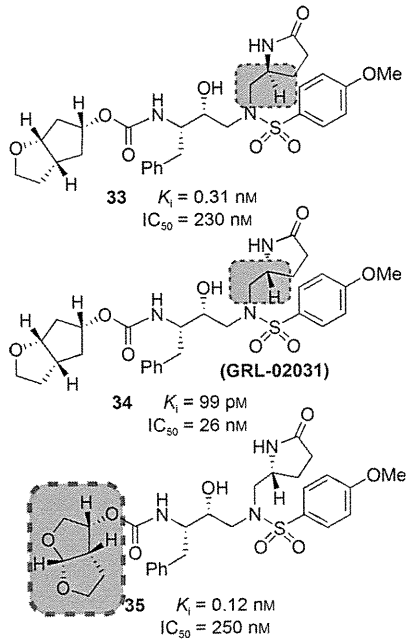

Figure 22. Structures and potency of PIs **33–35**.

showed good enzyme inhibitory potency but its antiviral IC_{50} value was 230 nM. The (*R*)-methyl-2-pyrrolidinone derivative **34** showed improvement in both the K_i value and antiviral activity (IC_{50} = 26 nM) relative to *S*-pyrrolidine derivative **33**. For the combination of bis-THF as P2 and (*R*)-methyl-2-oxazolidinone as P1′ ligands, however, the antiviral activity was significantly less than that of **10**. The antiviral potency of **34** was nearly ten times less than that of **23**. This is possibly a result of the poor cellular permeability of the polar 2-oxazolidinone functionality. Nevertheless, inhibitor **34** is a very potent inhibitor with antiviral activity comparable to that of FDA-approved PIs such as IDV, APV and LPV.[131]

To obtain molecular insight into various ligand binding site interactions, we determined a high-resolution X-ray crystal structure of **34**-bound HIV-1 protease at 1.29 Å resolution.[131] As shown in Figure 23 the interactions between the inhibitor and the active site are quite extensive. Most strikingly, the P1′-pyrrolidinone exists in two conformations. In one conformation, the pyrrolidinone NH group is engaged in a hydrogen bond with the Gly27′ carbonyl and the pyrrolidinone carbonyl forms a water-mediated hydrogen bond with the Arg8′ side chain. In another conformation, the pyrrolidinone ligand fills the hydrophobic pocket and the carbonyl group makes a weak hydrogen bond with the Val82′ backbone NH group. Other binding interactions of the Cp-THF ligand in the S2 site are similar to those of **23** and the methoxy oxygen in S2′ forms a strong hydrogen bond with the backbone NH group of Asp30′ and the side-chain carboxylate group.[131]

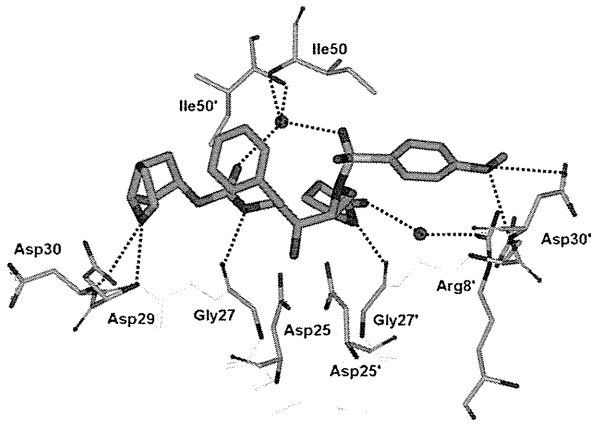

Figure 23. X-ray structure of **34**-bound HIV-1 protease.

Inhibitor **34** was evaluated against a wide spectrum of laboratory and clinical wild-type and multidrug-resistant HIV-1 strains. Table 13 shows its anti-HIV activity against selected clinical isolates highly resistant to multiple PIs.[131,132] As can be seen, inhibitor **34** was highly potent against various clinical isolates tested. Except darunavir, all other approved PIs failed to exert comparable activity. However, inhibitor **34**, like darunavir, potently inhibited all seven primary strains. Particularly, **34** maintained nearly full potency except with the R5 phenotype where it lost potency slightly (by less than twofold). Overall, the interactions of inhibitor **34** (GRL-02031) with backbone atoms particularly in the S1′ subsite were enhanced compared to those with inhibitor **23**. These polar interactions and the conformational flexibility of the P1′ oxazolidinone most likely contributed to its robust activity against multidrug-resistant HIV-1 variants.[132]

7. Conformationally Flexible P2 Ligands Capable of Forming Extensive Interactions with the Backbone

7.1. Design of Flexible Cyclic Polyethers as P2 Ligands and Their Effect on Drug-Resistance Properties

Following exploration of our PIs based on *meso* P2 ligands, we continued to examine ways in which we could reduce the stereochemical complexity of the bis-THF ligand while maintaining key backbone interactions and accommodating variations in the amino acid side chains within the active site occurring after viral mutations. To probe this, we turned to cyclic-polyether-derived P2 ligand systems possessing flexible rings capable of repacking within the binding pocket in response to mutational changes.[133] Based on this proposition, we removed the shared C–C bond from bis-THF producing the flexible eight-membered-ring inhibitor **36** shown in Figure 24. Unfortunately, **36** displayed significantly

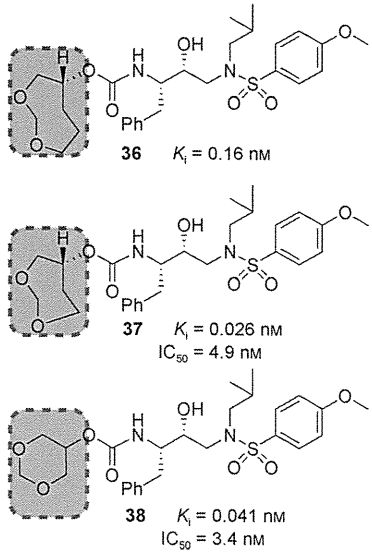

Figure 24. Structures and potency of PIs containing cyclic polyethers.

Table 13: Anti-HIV activity of **34** against selected clinical isolates highly resistant to multiple protease inhibitors.

Virus[a]	Phenotype	EC_{50} [μM]				
		IDV	APV	LPV	DRV	GRL-02031 (**34**)
HIV-$1_{ERS104pre}$ (wild-type)	X4	0.028	0.025	0.03	0.0036	0.028
HIV-1_{TM} (MDR)	X4	>1 (>36)	0.25 (10)	0.73 (24)	0.0036 (1)	0.029 (1)
HIV-1_{MM} (MDR)	R5	>1 (>36)	0.32 (13)	0.72 (24)	0.019 (5)	0.042 (2)
HIV-1_{C} (MDR)	X4	>1 (>36)	0.35 (14)	0.32 (11)	0.015 (4)	0.023 (1)
HIV-1_{G} (MDR)	X4	0.29 (10)	0.33 (13)	0.14 (5)	0.014 (4)	0.027 (1)

[a] Amino acid substitutions identified in the protease-encoding regions of HIV-$1_{ERS104pre}$, HIV-1_{TM}, HIV-1_{MM}, HIV-1_{C}, and HIV-1_{G} compared to the consensus B sequence cited from the Los Alamos database, see references [131] and [132].

lower enzyme inhibitory potency than darunavir. Reducing the ring size to a seven-membered ring restored enzyme inhibitory activity, and a preference for the *R* stereoisomer was revealed as the corresponding PI with epimeric P2 ligand displayed significant loss in potency ($K_i = 0.16$ nM, $IC_{50} = 30$ nM). Further reductions in ring size led to the six-membered-ring inhibitor **38** which was also highly potent. In general, expanding the ring to larger polycyclic ethers (ten-membered rings and larger) resulted in a drastic loss in potency. The ether oxygens within these ring systems are critical for maintaining high levels of enzyme inhibition activity. The removal of either oxygen from **37** resulted in a significant loss in activity.

An X-ray crystal structure of **37**-bound HIV-1 protease was determined at 1.00 Å resolution. The majority of binding interactions within the active site are similar in nature to those with inhibitor **10** (TMC-126) except for interactions in the S2 site. As shown in Figure 25, one of the oxygens of the 1,3-dioxepane ligand is involved in hydrogen bonding with Asp29 and Asp30 NH groups. The other oxygen is involved in a unique interaction with the Gly48 NH group through a water molecule.[133]

Both PIs **37** and **38** were further evaluated for their antiviral activity against a panel of clinically relevant HIV-1 isolates (Table 14). While they were less potent than darunavir, both compounds outperformed the approved PIs RTV and IDV and were comparable in antiviral activity to APV. These results suggested that the ability of the P2 ligand in **37** to maintain hydrogen-bonding interactions with the protein backbone may be responsible for the improved drug-resistance profiles of **37** over other PIs examined. The design of PIs using the concept of maximized backbone binding has led to PIs characterized by high potency against both wild-type and multidrug-resistant HIV-1 strains.[50]

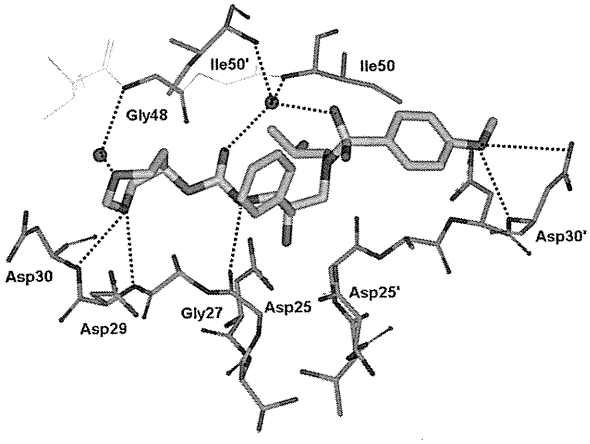

Figure 25. X-ray structure of **37**-bound HIV-1 protease.

7.2. Further Optimization of Bis-THF Ligands and the Design of a P2 TP-THF Ligand

We subsequently evaluated options to improve upon the bis-THF ligand of darunavir. An analysis of the X-ray structure of darunavir-bound HIV-1 protease (Figure 9) revealed that the bis-THF ether oxygens are involved in hydrogen-bonding interactions with the amide N-H groups of Asp29 and Asp30 at a distance of 2.9 and 3.1 Å, respectively. We conceptualized that incorporation of a larger ring system might promote closer more effective hydrogen bonding to these backbone residues and result in a more favorable alignment between the cyclic ether oxygen and the Asp30 amide N-H bond. These factors might result in stronger hydrogen bonds and higher affinity inhibitors. In addition, a larger ring size may promote favorable hydrophobic interactions within the S2 subsite and allow additional flexibility to better accommodate steric changes caused by protease mutations. Therefore, we synthesized and evaluated a series of PIs containing a tetrahydropyranyl-THF (Tp-THF) P2 ligand.[134] As shown in Figure 26, consistent with bis-THF, the bicyclic ligand in **39** (GRL-0476) with its 4*S* configuration is more effective than the epimeric ligand. Like the bis-THF ligand, both cyclic ether oxygens are critical for binding as their respective replacement with methylene groups resulted in a significant loss in potency. We have also prepared PIs **40** and **41** incorporating a *p*-methoxybenzyl side chain as the P1 ligand and *p*-methoxysulfonamide and *p*-aminophenylsulfonamide as the P2′ ligands, respectively. Our detailed drug-resistance studies of **40** and **41** showed that both PIs were very potent against multi-PI-resistant HIV-1 variants.[135]

To obtain molecular insight, we have created an active model of **39** starting from the X-ray crystal structure of **10** (TMC-126). The conformation of **39** was optimized using the

Table 14: Anti-HIV activity of **37** and **38** against selected clinical isolates highly resistant to multiple protease inhibitors.

Virus[a]	IC_{50} [nM] values					
	IDV	RTV	APV	DRV	**37**	**38**
ERS104pre (wild-type)	26	34	33	3.5	20	6
MDR/TM	>1000 (>38)	>1000 (>29)	290 (9)	4 (1)	220 (11)	64 (10)
MDR/MM	>1000 (>38)	>1000 (>29)	300 (9)	17 (5)	250 (13)	110 (5)
MDR/JSL	>1000 (>38)	>1000 (>29)	430 (13)	26 (7)	500 (25)	330 (55)
MDR/B	>1000 (>38)	>1000 (>29)	320 (10)	26 (7)	340 (17)	230 (38)
MDR/C	>1000 (>38)	>1000 (>29)	230 (7)	7 (2)	210 (11)	160 (27)
MDR/G	290 (11)	>1000 (>29)	340 (10)	7 (2)	360 (18)	300 (50)
MDR/A	>1000 (>38)	>1000 (>29)	100 (3)	3 (1)	20 (1)	13 (2)

[a] Amino acid substitutions identified in the protease-encoding region compared to the consensus type B sequence cited from the Los Alamos database, see reference [133].

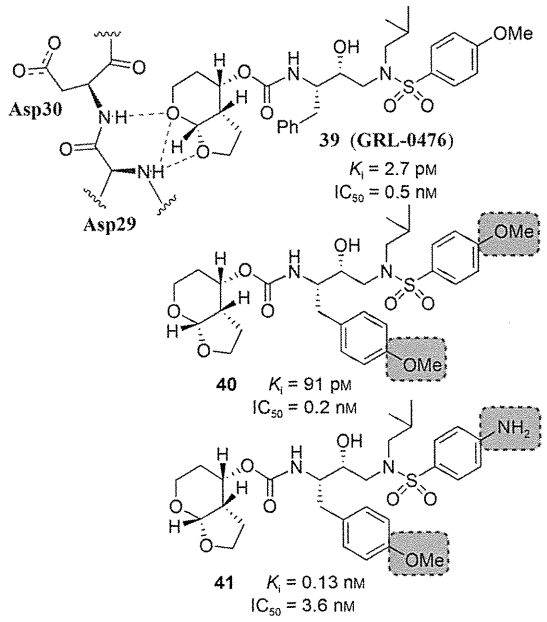

Figure 26. Structure and potency of Tp-THF-derived PIs.

MMFF94 force field.[136] It appeared that the cyclic ether oxygens of Tp-THF are within hydrogen-bonding distance to Asp29 and Asp30 backbone NH groups in the S2 subsite. Other active-site interactions are similar to those in the X-ray structure of **10**-bound HIV-1 protease.[95] As depicted in Table 15, against a panel of multidrug-resistant clinical isolates, inhibitor **39** outperformed two other approved PIs (APV and LPV) displaying a high level of antiviral activity against all the strains with EC_{50} values ranging from 2.6 to 27.5 nM. These results are comparable to those of **10** (TMC-126), and **39** is more potent than darunavir in absolute terms; however, the fold changes in efficacy factors between viral strains are similar.

8. Further Improvement of Drug Resistance by Targeting Protein Backbone and Protein–Ligand Interactions

In our efforts to target the protein backbone as a design strategy to combat drug resistance, we have developed a variety of intriguing ligands and scaffolds and generated diverse inhibitors with exceptional potency and drug-resistance profiles. Our next objective was to further optimize a ligand structure that could maintain critical backbone interactions and at the same time effectively fill the hydrophobic pocket in the active site and maximize protein–ligand interactions. Towards this objective, we elected to append functionalities to the bis-THF ligand to further improve the drug-resistance properties of the PIs. As shown in Figure 27, based upon the overlay of the X-ray structures of darunavir-bound[69] and SQV-bound[86] HIV-1 protease, we planned to

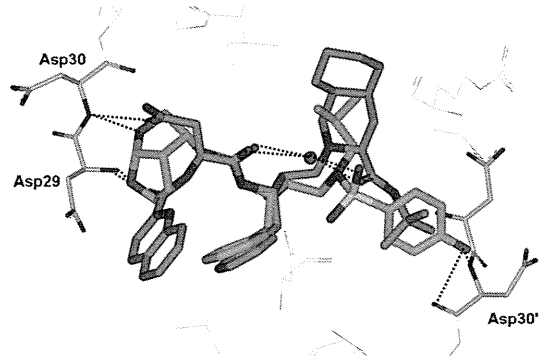

Figure 27. Overlay of the X-ray structures of darunavir-bound and SQV-bound HIV-1 protease.

fill the hydrophobic pocket occupied by the quinaldic moiety of SQV. Particularly, we have speculated that the fusion of another tetrahydrofuran ring on the bis-THF ligand would provide additional ligand binding site interactions. While such an oxatricyclic ligand could have a number of possible stereochemical motifs, including *syn-syn-syn* (*SSS*-type) and *syn-anti-syn* (*SAS*-type) isomers, our model based upon overlay structures in Figure 27 suggested that the *SAS*-type ligand-based inhibitor would make enhanced interactions in the S2 subsite. We subsequently synthesized both *SAS*- and *SSS*-oxatricyclic ligands in a stereoselective manner and prepared the respective PIs **42** and **43** shown in Figure 28.[137]

Inhibitor **42** (GRL-0519A) with the *syn-anti-syn* configuration of the tris-THF rings exhibited a tenfold better enzyme inhibitory potency over the *syn-syn-syn* derivative **43**. Inhibitor **42** also displayed better antiviral activity than **43**. An X-ray structure of **42**-bound HIV-1 protease was determined at 1.27 Å (Figure 29).[137] Analysis of this structure revealed a

Table 15: Comparison of the antiviral activity of **39** against multidrug-resistant clinical isolates.

Virus[a]	Phenotype	EC_{50} [μM]			
		ATV	LPV	DRV	**39** (GRL-0476)
$HIV\text{-}1_{ERS104pre}$ (wild type)	X4	0.0027	0.031	0.004	0.0019
$HIV\text{-}1_{MDR/B}$	X4	0.470 (174)	>1 (>32)	0.034 (9)	0.0145 (8)
$HIV\text{-}1_{MDR/C}$	X4	0.039 (14)	0.437 (14)	0.009 (2)	0.0037 (2)
$HIV\text{-}1_{MDR/G}$	X4	0.019 (7)	0.181 (6)	0.026 (7)	0.0026 (1)
$HIV\text{-}1_{MDR/TM}$	X4	0.075 (28)	0.423 (14)	0.022 (6)	0.0275 (14)
$HIV\text{-}1_{MDR/MM}$	R5	0.205 (76)	0.762 (25)	0.017 (4)	0.0050 (3)
$HIV\text{-}1_{MDR/JSL}$	R5	0.293 (109)	>1 (>32)	0.023 (6)	0.0275 (14)

[a] For details of amino acid substitutions identified in the protease-encoding region of $HIV\text{-}1_{ERS104pre}$, $HIV\text{-}1_{B}$, $HIV\text{-}1_{C}$, $HIV\text{-}1_{G}$, $HIV\text{-}1_{TM}$, $HIV\text{-}1_{MM}$, and $HIV\text{-}1_{JSL}$ and the assay protocol, see references [134] and [135].

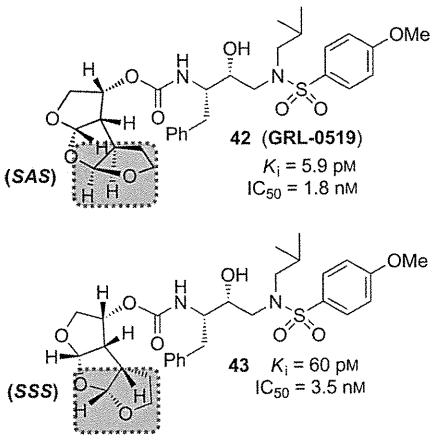

Figure 28. Structures and potency of PIs **42** and **43**.

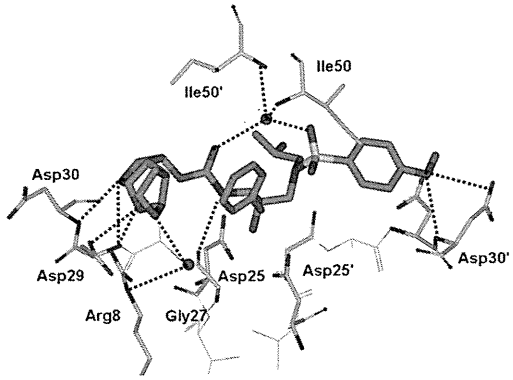

Figure 29. X-ray structure of **42**-bound HIV protease (PDB code 30K9).[137]

number of additional interactions within the S2 subsite not seen with the bis-THF unit of darunavir or TMC-126. The two top THF ring oxygens are involved in hydrogen-bonding interactions with the backbone NH groups of Asp29 and Asp30. The second THF oxygen appears to form a hydrogen bond with the carboxylate side chain of Asp29. As expected, the third THF ring fills the S2 subsite very nicely. The third THF ring also participates in a semicircular hydrogen-bonding network with three conserved water molecules that surround the guanidine side chain of Arg8.

Inhibitor **42** proved to be extremely potent against various multidrug-resistant HIV-1 variants, with IC_{50} values ranging from 0.6–4.3 nM, nearly a 10-fold improvement over the potency of darunavir (Table 16). The emergence of GRL-0519A-resistant HIV-1 in vitro was substantially delayed compared to selected approved PIs.[137] Also, very strikingly, GRL-0519A more potently blocked protease dimerization by at least a factor of 10 compared to darunavir as examined in the fluorescence resonance energy transfer based HIV-1 expression assay employing cyan and yellow fluorescent protein tagged protease monomers.[112] The present data suggested that the GRL-0519 class of PIs may be further developed as potential therapeutic agents for the treatment of primary and multidrug-resistant HIV-1 infections.

Table 16: Antiviral activity of **42**, amprenavir (APV), and darunavir (DRV) against multidrug-resistant clinical isolates in PHA-PBMCs.

Virus[a]	EC50 [μm]		
	APV	DRV	**42** (GRL-0519)
$HIV\text{-}1_{ERS104pre}$ (wild-type)	0.032	0.005	0.0006
$HIV\text{-}1_{MDR/B}$	0.521 (16)	0.028 (6)	0.0043 (7)
$HIV\text{-}1_{MDR/C}$	0.357 (11)	0.011 (2)	0.0009 (2)
$HIV\text{-}1_{MDR/G}$	0.485 (15)	0.031 (6)	0.0027 (5)
$HIV\text{-}1_{MDR/TM}$	0.488 (15)	0.031 (6)	0.0022 (4)
$HIV\text{-}1_{MDR/MM}$	0.291 (9)	0.016 (3)	0.0027 (5)
$HIV\text{-}1_{MDR/JSL}$	0.419 (13)	0.024 (5)	0.0028 (5)

[a] See reference [137] for details.

9. Summary and Outlook

Our specific interest in the chemistry and biology of natural products brought a unique perspective to our design and synthesis of HIV-1 protease inhibitors for the treatment of HIV infection and AIDS. Our initial academic pursuit was focused on addressing the question of whether we could design natural product derived ligands or templates that could mimic the biological mode of action of peptide bonds and alleviate problems inherent to peptide-based drugs. Nature has been optimizing various cyclic ether/polycyclic ether templates for millions of years in various biological micro-environments involving biosynthetic enzymes. Inspired by nature and based upon X-ray structures of protein–ligand complexes, we invoked the idea of designing stereochemically defined cyclic ether or polyether-like molecular features to replace peptide bonds and effectively fill the hydrophobic pockets in the active site of HIV-1 protease. We envisioned positioning cyclic ether oxygen to mimic the biological action of a peptide carbonyl group and the cyclic functionality would make necessary van der Waals interactions in the hydrophobic pocket. These research efforts led to the creation of a variety of conceptually novel molecular templates that are entirely nonpeptidic but interact with HIV-1 protease with remarkable affinity. Our many X-ray structural studies of inhibitor-bound HIV-1 proteases provided strong evidence that such a cyclic ether/polyether oxygen indeed serves as an effective mimic of the carbonyl of a peptide/amide functionality. Also, such cyclic units nicely fill the hydrophobic pockets in the enzyme active site.

Following the development of various nonpeptide high-affinity ligands, we turned toward addressing the issue of drug resistance. We were interested in optimizing inhibitor structures against wild-type HIV-1 protease as well as against known mutant proteases. This objective led us to examine X-ray structures of inhibitor-bound wild-type HIV-1 proteases as well as the X-ray structures of a number of mutant proteases. Superimposition of these X-ray structures evidenced only minimal distortion of the backbone conformation. This led to our proposition of targeting the protein backbone as a strategy to evade drug resistance. By maximizing hydrogen-bonding interactions with the protein backbone, we have essentially created a "molecular crab" capable of latching on and holding tightly in the enzyme active site.

Using the combination of our in-depth antiviral studies, along with drug-resistance, and X-ray crystallographic studies, we have documented the practicality and usefulness of the backbone-binding design strategy to combat drug resistance. The combination of our ligand-design efforts inspired by polyether natural products, and subsequent inhibitor design efforts targeting the protease backbone to combat drug resistance, culminated in the discovery and ultimate development of darunavir, the first FDA-approved treatment for patients with multidrug-resistant HIV-1 variants. Its indications were later generalized for all patients with HIV infection and AIDS. Furthermore, we discovered that darunavir possesses a dual mechanism of action and is a potent inhibitor of HIV-1 protease dimerization.

The discovery of darunavir marked an important turning point in the paradigm of designing HIV PIs. Our work has led us to develop the backbone-binding concept as an effective means to mitigate viral adaptability. We have continued to apply our backbone-binding design strategy resulting in the design and synthesis of a variety of exceedingly potent HIV-1 protease inhibitors with intriguing structural features. Interestingly, GRL-02031 retained near full potency against a panel of multidrug-resistant HIV-1 variants. Also, the design of GRL-0519 marked a tenfold improvement in antiviral activity over that of darunavir with retention of potency against a wide range of clinically relevant multidrug-resistant strains. The backbone-binding concept may prove useful as a guide for the design of antiretroviral agents in other areas as well. We will continue to utilize and develop this concept in our future designs as we strive to meet the challenges of today's medicine.

This work was supported by the National Institute of Health (GM53386). We thank Dr. K. V. Rao (Purdue University) for helpful discussions.

Received: April 20, 2011
Published online: January 31, 2012

[1] E. Domingo, C. K. Biebricher, M. Eigen, J. J. Holland in *Quasispecies and RNA Virus Evolution: Principles and Consequences*, Eurekah, Georgetown, **2001**, preface.
[2] M. Burnet, D. O. White in *Natural History of Infectious Disease*, Cambridge University Press, London, **1972**.
[3] J. Needham, L. Gwei-djen in *Science and Civilization in China, Vol. 6* (Ed.: N. Sivin), Cambridge University Press, Cambridge, **1999**, p. 134.
[4] A. Waterson, L. Wilkinson in *An Introduction to the History of Virology*, Cambridge University Press, Cambridge, **1978**, pp. 23–34.
[5] F. Fenner, F. M. Burnett in *Portraits of Viruses: A History of Virology* (Eds.: F. Fenner, A. Gibbs), S. Karger AG, Basel, **1988**, pp. 1–37.
[6] J. B. Brooksby in *Portraits of Viruses: A History of Virology* (Eds.: F. Fenner, A. Gibbs), S. Karger AG, Basel, **1988**, pp. 124–146.
[7] WHO, Summary of SARS Cases, http://www.who.int/csr/sars/country/country2003_08_15.pdf, **2003**.
[8] WHO, Cumulative Number of Confirmed Human Cases of Avian Influenza A/(H5N1) Reported to WHO, http://www.who.int/csr/disease/avian_influenza/country/cases_table_2011_02_02/en/index.htm, **2011**.
[9] UNAIDS Report on the global HIV/AIDS epidemic, http://www.unaids.org/en/media/unaids/contentassets/documents/unaidspublication/2010/20101123_globalreport_en.pdf, **2010**.
[10] F. Barre-Sinoussi, J. Chermann, F. Rey, M. Nugeyre, S. Chamaret, J. Gruest, C. Dauguet, C. Axler-Blin, et al., *Science* **1983**, *220*, 868–871.
[11] R. C. Gallo, P. S. Sarin, E. P. Gelmann, M. Robert-Guroff, E. Richardson, V. S. Kalyanaraman, D. Mann, G. D. Sidhu, R. E. Stahl, S. Zolla-Pazner, J. Leibowitch, M. Popovic, *Science* **1983**, *220*, 865–867.
[12] T. Lyle in *Comprehensive Medicinal Chemistry II, Vol. 7* (Eds.: J. Taylor, D. Triggle), Elsevier Science Maryland Heights, **2007**, pp. 329–371.
[13] Y. Mehellou, E. De Clercq, *J. Med. Chem.* **2010**, *53*, 521–538.
[14] L. Menéndez-Arias, *Antiviral Res.* **2010**, *85*, 210–231.
[15] C. Flexner, *Nat. Rev. Drug Discovery* **2007**, *6*, 959–966.
[16] H. Mitsuya, S. Broder, *Nature* **1987**, *325*, 773–778.
[17] N. E. Kohl, E. A. Emini, W. A. Schleif, L. J. Davis, J. C. Heimbach, R. A. F. Dixon, E. M. Scolnick, I. S. Sigal, *Proc. Natl. Acad. Sci. USA* **1988**, *85*, 4686–4690.
[18] S. Virgil in *Methods and Principles in Medicinal Chemistry, Vol. 45* (Ed.: A. K. Ghosh), Wiley-VCH, Weinheim, **2010**, pp. 139–168.
[19] H. Mitsuya, J. Erickson in *Textbook of AIDS Medicine* (Eds.: T. Merigan, J. Bartlett, D. Bolgnesi), Williams & Wilkis, Baltimore, **1999**, pp. 751–780.
[20] M. Glesby in *Protease Inhibitors in AIDS Therapy*, (Eds.: R. Ogden, C. Flexner), Marcel Dekker, New York, **2001**, pp. 237–256.
[21] A. Wensing, N. M. van Maarseveen, M. Nijhuis, *Antiviral Res.* **2010**, *85*, 59–74.
[22] S. Grabar, C. Pradier, E. Le Corfec, R. Lancar, C. Allavena, M. Bentata, P. Berlureau, C. Dupont, P. Fabbro-Peray, I. Poizot-Martin, D. Costagliola, *AIDS* **2000**, *14*, 141–149.
[23] M. Wainberg, G. Friedland, *JAMA J. Am. Med. Assoc.* **1998**, *279*, 1977–1983.
[24] L. Mansky, H. Temin, *J. Virol.* **1995**, *69*, 5087–5094.
[25] J. Drake, J. Holland, *Proc. Natl. Acad. Sci. USA* **1999**, *96*, 13910–13913.
[26] A. Perelson, A. Neumann, M. Markowitz, J. Leonard, D. Ho, *Science* **1996**, *271*, 1582–1586.
[27] D. Robertson, B. Hahn, P. Sharp, *J. Mol. Evol.* **1995**, *40*, 249–259.
[28] A. Leigh Brown, *Proc. Natl. Acad. Sci. USA* **1997**, *94*, 1862–1865.
[29] R. Steigbigel, D. Cooper, P. Kumar, et al., *N. Engl. J. Med.* **2008**, *359*, 339–354.
[30] J. Stephenson, *J. Am. Med. Assoc.* **2007**, *297*, 1535–1536.
[31] P. Cane, J. Antimicro, *Chemoth* **2009**, *Suppl. 1*, i37–i40.
[32] B. Dau, M. Holodniy, *Drugs* **2009**, *69*, 31–50.
[33] C. Stoddart, P. Joshi, B. Sloan, J. Bare, P. Smith, G. Allaway, C. Wild, D. Martin, *PLoS ONE* **2007**, *2*, e1251.
[34] J. Tazi, N. Bakkour, V. Marchand, L. Ayadi, A. Aboufirassi, C. Branlant, *FEBS J.* **2010**, *277*, 867–876.
[35] H. Mitsuya, A. Ghosh in *Aspartic Acid Proteases as Therapeutic Targets* (Ed.: A. Ghosh), Wiley-VCH, Weinheim, **2010**, pp. 245–262.
[36] E. Domingo, R. Webster, J. Holland in *Origins and Evolution of Viruses*, Academic Press, London, **1999**, pp. 197–224.
[37] A. Ali, R. Bandaranayake, Y. Cai, N. King, M. Kolli, S. Mittal, J. Murzycki, M. Nalam, E. Nalivaika, A. Ozen, M. Prabu-Jeyabalan, K. Thayer, C. Schiffer, *Viruses* **2010**, *2*, 2509–2535.
[38] L. Menéndez-Arias, *Antiviral Res.* **2010**, *85*, 210–231.
[39] A. Wensing, N. Maarseveen, M. Nijhuis, *Antiviral Res.* **2010**, *59–74*.

[40] S. V. Gulnik, L. I. Suvorov, B. Liu, B. Yu, B. Anderson, H. Mitsuya, J. W. Erickson, *Biochemistry* **1995**, *34*, 9282–9287.
[41] R. Kantor, W. J. Fessel, A. R. Zolopa, D. Israelski, N. Shulman, J. G. Montoya, M. Harbour, J. M. Schapiro, R. W. Shafer, *Antimicrob. Agents Chemother.* **2002**, *46*, 1086–1092.
[42] K. Yusa, W. Song, M. Bartelmann, S. Harada, *J. Virol.* **2002**, *76*, 3031–3037.
[43] G. Croteau, L. Doyon, D. Thibeault, G. McKercher, L. Pilote, D. Lamarre, *J. Virol.* **1997**, *71*, 1089–1096.
[44] J. Martinez-Picado, A. V. Savara, L. Sutton, R. T. D'Aquila, *J. Virol.* **1999**, *73*, 3744–3752.
[45] J. Condra, W. Schleif, O. Blahy, L. Gabryelski, D. J. Graham, J. C. Quintero, A. Rhodes, H. L. Robbins, E. Roth, M. Shivaprakash, D. Titus, T. Yang, H. Tepplert, K. E. Squires, P. J. Deutsch, E. A. Emini, *Nature* **1995**, *374*, 569–571.
[46] S. Tamiya, S. Mardy, M. Kavlick, K. Yoshimura, H. Mitsuya, *J. Virol.* **2004**, *78*, 12030–12040.
[47] F. Mammano, C. Petit, F. Clavel, *J. Virol.* **1998**, *72*, 7632–7637.
[48] L. Hong, X. Zhang, J. A. Hartsuck, J. Tang, *Protein Sci.* **2000**, *9*, 1898–1904.
[49] G. S. Laco, C. Schalk-Hihi, J. Lubkowski, G. Morris, A. Zdanov, A. Olson, J. H. Elder, A. Wlodawer, A. Gustchina, *Biochemistry* **1997**, *36*, 10696–10708.
[50] A. K. Ghosh, B. Chapsal, I. Weber, H. Mitsuya, *Acc. Chem. Res.* **2008**, *41*, 78–86.
[51] A. K. Ghosh, P. R. Sridhar, S. Leshchenko, A. K. Hussain, J. Li, A. Y. Kovalevsky, D. E. Walters, J. Wedekind, V. Grum-Tokars, D. Das, Y. Koh, K. Maeda, H. Gatanaga, I. T. Weber, H. Mitsuya, *J. Med. Chem.* **2006**, *49*, 5252–5261.
[52] J. Agniswamy, I. T. Weber, *Viruses* **2009**, *1*, 1110–1136.
[53] A. Wlodawer, J. Vondrasek, *Annu. Rev. Biophys. Biomol. Struct.* **1998**, *27*, 249–284.
[54] C. Chothia, A. Lesk, *Cold Spring Harbor Symp. Quant. Biol.* **1987**, *52*, 399–405.
[55] C. Worth, S. Gong, T. Blundell, *Nat. Rev. Mol. Cell Biol.* **2009**, *10*, 709–720.
[56] A. Todd, C. Orengo, J. Thornton, *Curr. Opin. Chem. Biol.* **1999**, *3*, 548–556.
[57] J. Liang, H. Edelsbrunner, C. Woodward, *Protein Sci.* **1998**, *7*, 1884–1897.
[58] R. Wolfenden, M. J. Snider, *Acc. Chem. Res.* **2001**, *34*, 938–945.
[59] S. J. Benkovic, S. Hammes-Schiffer, *Science* **2003**, *301*, 1196–1202.
[60] M. Garcia-Viloca, J. Gao, M. Karplus, D. G. Truhlar, *Science* **2004**, *303*, 186–195.
[61] A. Wlodawer, M. Miller, M. Jaskolski, B. K. Sathyanarayana, E. Baldwin, I. T. Weber, L. M. Selk, L. Clawson, J. Schneider, S. B. Kent, *Science* **1989**, *245*, 616–621.
[62] A. Gustchina, I. T. Weber, *FEBS Lett.* **1990**, *269*, 269–272.
[63] A. Gustchina, C. Sansom, M. Prevost, J. Richelle, S. Y. Wodak, A. Wlodawer, I. T. Weber, *Protein Eng.* **1994**, *7*, 309–317.
[64] Y. Tie, P. I. Boross, Y. F. Wang, L. Gaddis, F. Liu, X. Chen, J. Tozser, R. W. Harrison, I. T. Weber, *FEBS J.* **2005**, *272*, 5265–5277.
[65] A. Wlodawer, A. Gustchina, *Biochim. Biophys. Acta Protein Struct. Mol. Enzymol.* **2000**, *1477*, 16–34.
[66] W. Wang, P. A. Kollman, *Proc. Natl. Acad. Sci. USA* **2001**, *98*, 14937–14942.
[67] A. K. Ghosh, P. R. Sridhar, N. Kumaragurubaran, Y. Koh, I. T. Weber, H. Mitsuya, *ChemMedChem* **2006**, *1*, 939–950.
[68] A. K. Ghosh, *J. Med. Chem.* **2009**, *52*, 2163–2176.
[69] A. Y. Kovalevsky, F. Liu, S. Leshchenko, A. K. Ghosh, J. M. Louis, R. W. Harrison, I. T. Weber, *J. Mol. Biol.* **2006**, *363*, 161–173.
[70] F. Liu, P. I. Boross, Y. F. Wang, J. Tozser, J. M. Louis, R. W. Harrison, I. T. Weber, *J. Mol. Biol.* **2005**, *354*, 789–800.
[71] A. Y. Kovalevsky, Y. Tie, F. Liu, P. I. Boross, Y. F. Wang, S. Leshchenko, A. K. Ghosh, R. W. Harrison, I. T. Weber, *J. Med. Chem.* **2006**, *49*, 1379–1387.
[72] F. Liu, A. Y. Kovalevsky, J. M. Louis, P. I. Boross, Y. F. Wang, R. W. Harrison, I. T. Weber, *J. Mol. Biol.* **2006**, *358*, 1191–1199.
[73] B. Mahalingam, Y. F. Wang, P. I. Boross, J. Tozser, J. M. Louis, R. W. Harrison, I. T. Weber, *Eur. J. Biochem.* **2004**, *271*, 1516–1524.
[74] Y. Tie, A. Y. Kovalevsky, P. Boross, Y. F. Wang, A. K. Ghosh, J. Tozser, R. W. Harrison, I. T. Weber, *Proteins Struct. Funct. Bioinf.* **2007**, *67*, 232–242.
[75] P. Martin, J. F. Vickrey, G. Proteasa, Y. L. Jimenez, Z. Wawrzak, M. A. Winters, T. C. Merigan, L. C. Kovari, *Structure* **2005**, *13*, 1887–1895.
[76] C. H. Shen, Y. F. Wang, A. Y. Kovalevsky, R. W. Harrison, I. T. Weber, *FEBS J.* **2010**, *277*, 3699–3714.
[77] J. F. Miller, C. W. Andrews, M. Brieger, E. S. Furfine, M. R. Hale, M. H. Hanlon, R. J. Hazen, I. Kaldor, et al., *Bioorg. Med. Chem. Lett.* **2006**, *16*, 1788–1794.
[78] J. C. Clemente, R. E. Moose, R. Hemrajani, L. R. Whitford, L. Govindasamy, R. Reutzel, R. McKenna, M. Agbandje-McKenna, M. M. Goodenow, B. M. Dunn, *Biochemistry* **2004**, *43*, 12141–12151.
[79] Z. Chen, Y. Li, E. Chen, D. L. Hall, P. L. Darke, C. Culberson, J. A. Shafer, L. C. Kuo, *J. Biol. Chem.* **1994**, *269*, 26344–26348.
[80] A. K. Ghosh, S. Gemma, E. Simoni, A. Baldridge, D. E. Waters, K. Ide, Y. Tojo, Y. Koh, H. Mitsuya, *Bioorg. Med. Chem. Lett.* **2010**, *20*, 1241–1246.
[81] A. K. Ghosh, J. F. Kincaid, W. Cho, D. E. Walters, K. Krishnan, K. A. Hussain, Y. Koo, H. Cho, C. Rudall, L. Holland, J. Buthod, *Bioorg. Med. Chem. Lett.* **1998**, *8*, 687–690.
[82] K. Yoshimura, R. Kato, M. F. Kavlck, A. Nguyen, V. Maroun, K. Maeda, K. A. Hussain, A. K. Ghosh, S. V. Gulnik, J. W. Erickson, H. Mistuya, *J. Virol.* **2002**, *76*, 1349–1358.
[83] A. K. Ghosh, Z. L. Dawson, H. Mitsuya, *Bioorg. Med. Chem.* **2007**, *15*, 7576–7580.
[84] A. K. Ghosh, B. D. Chapsal, H. Mitsuaya in *Aspartic Acid Proteases as Therapeutic Targets* (Ed.: A. K. Ghosh), Wiley-VCH, Weinheim, **2010**, pp. 205–235.
[85] N. A. Roberts, J. A. Martin, D. Kinchington, A. V. Broadhurst, J. C. Craig, I. B. Duncan, S. A. Galpin, B. K. Handa, J. Kay, A. Krohn, R. W. Lambert, J. H. Merrett, J. S. Mills, K. E. B. Parkes, S. Redshaw, A. J. Ritchie, D. L. Taylor, G. J. Thomas, P. J. Machin, *Science* **1990**, *248*, 358–361.
[86] A. Krohn, S. Redshaw, J. C. Ritchie, B. J. Graves, M. H. Hatada, *J. Med. Chem.* **1991**, *34*, 3340–3342.
[87] K. Nakanishi, *Bioorg. Med. Chem.* **2005**, *13*, 4987–5000.
[88] A. L. Donoho, *J. Anim. Sci.* **1984**, *58*, 1528–1539.
[89] A. K. Ghosh, W. J. Thompson, M. K. Holloway, S. P. McKee, T. T. Duong, H. Y. Lee, P. M. Munson, A. M. Smith, J. M. Wai, P. L. Darke, et al., *J. Med. Chem.* **1993**, *36*, 2300–2310.
[90] A. K. Ghosh, W. J. Thompson, S. P. McKee, T. T. Duong, T. A. Lyle, J. C. Chen, P. L. Darke, J. A. Zugay, E. A. Emini, W. A. Schleif, et al., *J. Med. Chem.* **1993**, *36*, 292–294.
[91] M. L. Vazquez, M. L. Bryant, M. Clare, G. A. DeCrescenzo, E. M. Doherty, J. N. Freskos, D. P. Getman, K. A. Houseman, J. A. Julien, G. P. Kocan, *J. Med. Chem.* **1995**, *38*, 581–584.
[92] R. D. Tung, D. J. Livingston, B. G. Rao, E. E. Kim, C. T. Baker, J. S. Boger, S. P. Chambers, D. D. Deininger, M. Dwyer, L. Elsayed, J. Fulghum, B. Li, M. A. Murcko, M. A. Navia, P. Novak, S. Pazhanisamy, C. Stuver, J. A. Thomson in *Protease Inhibitors in AIDS* Therapy (Eds.: R. C. Ogden, C. W. Flexner), Marcel Dekker, New York, **2001**, pp. 101–137.
[93] E. E. Kim, C. T. Baker, M. D. Dwyer, M. A. Murcko, B. G. Rao, R. D. Tung, M. A. Navia, *J. Am. Chem. Soc.* **1995**, *117*, 1181–1182.

[94] A. K. Ghosh, J. F. Kincaid, D. E. Walters, Y. Chen, N. C. Chaudhuri, W. J. Thompson, C. Culberson, P. M. Fitzgerald, H. Y. Lee, S. P. McKee, P. M. Munson, T. T. Duong, P. L. Darke, J. A. Zugay, W. A. Schleif, M. G. Axel, J. Lin, J. R. Huff, *J. Med. Chem.* **1996**, *39*, 3278–3290.

[95] A. K. Ghosh, S. Kulkarni, D. D. Anderson, L. Hong, A. Baldridge, Y.-F. Wang, A. A. Chumanevich, A. Y. Kovalevsky, Y. Tojo, M. Amano, Y. Koh, J. Tang, I. T. Weber, H. Mitsuya, *J. Med. Chem.* **2009**, *52*, 7689–7705.

[96] J. W. Erickson, S. V. Gulnik, H. Mitsuya, A. K. Ghosh (Fitness Assay and Associated Methods), US Patent 7470506B1, **2008**.

[97] S. De Meyer, M. Peters, Abstracts 533 and 620, *11th Conference on Retroviruses and Opportunistic Infections (CROI)*, February 8–11 **2004**, San Francisco, CA (USA).

[98] R. Hoetelmans, I. van der Sandt, M. De Pauw, K. Struble, M. Peeters, R. van der Geest, Abstract 549, *10th Conference on Retroviruses and Opportunistic Infections (CROI)*, February **2003**, Boston, MA (USA).

[99] D. L. Surleraux, A. Tahri, W. G. Verschueren, G. M. Pille, H. A. De Kock, T. H. Jonckers, A. Peeters, S. De Meyer, H. Azjin, R. Pauwels, M. P. de Bethune, N. M. King, M. Prabu-Jeyabalan, C. A. Schiffer, P. B. Wigerinck, *J. Med. Chem.* **2005**, *48*, 1813–1822.

[100] Y. Tie, P. Boross, Y. Wang, L. Gaddis, A. Hussain, S. Leshchenko, A. Ghosh, J. Louis, R. Harrison, I. Weber, *J. Mol. Biol.* **2004**, *338*, 341–352.

[101] N. King, M. Prabu-Jeyabalan, E. Nalivaika, P. Wigerinck, M. de Bethune, C. Schiffer, *J. Virol.* **2004**, *78*, 12012–12021.

[102] I. Dierynck, I. Keuleers, M. De Wit, A. Tahri, D. Surleraux, D. A. Peeters, K. Hertogs, *Antiviral Res.* **2005**, *10*, S71.

[103] E. Lefebvre, C. Schiffer, *AIDS Rev.* **2008**, *10*, 131–142.

[104] A. Kovalevsky, A. K. Ghosh, I. T. Weber, *J. Med. Chem.* **2008**, *51*, 6599–6603.

[105] Y. Koh, H. Nakata, K. Maeda, H. Ogata, H. G. Bilcer, T. Devasamudram, J. F. Kincaid, P. Boross, Y. F. Wang, Y. Tie, P. Volarath, L. Gaddis, R. W. Harrison, I. T. Weber, A. K. Ghosh, H. Mitsuya, *Antimicrob. Agents Chemother.* **2003**, *47*, 3123–3129.

[106] S. De Meyer, H. Azijn, D. Surleraux, D. Jochmans, A. Tahri, R. Pauwels, P. Wigerinck, M. de Bethune, *Antimicrob. Agents Chemother.* **2005**, *49*, 2314–2321.

[107] Y. Koh, M. Amano, T. Towata, M. Danish, S. Leshchenko-Yashchuk, D. Das, M. Nakayama, Y. Tojo, A. K. Ghosh, H. Mitsuya, *J. Virol.* **2010**, *84*, 11961–11969.

[108] S. De Meyer, A. Hill, I. De Baere, I. Rimsky, H. Azijin, B. Van Baelen, E. De Paepe, T. Vangeneugden, et al., *Antiviral Ther.* **2006**, *11*, S73.

[109] C. Wolfe, C. Hicks, *HIV/AIDS* **2009**, *1*, 13–21.

[110] K. Saskova, M. Kozisek, P. Rezacova, J. Brynda, T. Yashina, R. Kagan, J. Konvalinka, *J. Virol.* **2009**, *83*, 8810–8818.

[111] A. Wlodwaer, M. Miller, M. Jaskolski, B. Sathyanarayana, E. Baldwin, I. Weber, L. Selk, L. Clawson, *Science* **1989**, *245*, 616–621.

[112] Y. Koh, S. Matsumi, D. Das, M. Amano, D. Davis, J. Li, S. Leschenko, A. Baldridge, et al., *J. Biol. Chem.* **2007**, *282*, 28709–28720.

[113] M. Amano, Y. Koh, D. Das, J. Li, S. Leschenko, Y. F. Wang, P. I. Boross, I. T. Weber, A. K. Ghosh, H. Mitsuya, *Antimicrob. Agents Chemother.* **2007**, *51*, 2143–2155.

[114] Y. F. Wang, Y. Tie, P. I. Boross, J. Tozser, A. K. Ghosh, R. W. Harrison, I. T. Weber, *J. Med. Chem.* **2007**, *50*, 4509–4515.

[115] J. F. Miller, E. S. Furfine, M. H. Hanlon, R. J. Hazen, J. A. Ray, L. Robinson, V. Samano, A. Spaltenstein, *Bioorg. Med. Chem. Lett.* **2004**, *14*, 959–963.

[116] R. Hazen, R. Harvey, R. Ferris, C. Craig, P. Yates, P. Griffin, J. Miller, I. Kaldor, J. Ray, V. Samano, E. Furfine, A. Spaltenstein, M. Hale, R. Tung, M. St. Clair, M. Hanlon, L. Boone, *Antimicrob. Agents Chemother.* **2007**, *51*, 3147–3154.

[117] S. L. Ford, Y. S. Reddy, M. T. Anderson, S. C. Murray, P. Fernandez, D. S. Stein, M. A. Johnson, *Antimicrob. Agents Chemother.* **2006**, *50*, 2201–2206.

[118] J. R. Lalezari, D. J. Ward, S. A. Tomkin, H. R. Garges, *J. Antimicrob. Chemother.* **2007**, *60*, 170–174.

[119] Corresponding press release online: "GlaxoSmithKline Discontinues Clinical Development of Investigational Protease Inhibitor Brecanavir (640385)". http://www.gsk.com/media/pressreleases/2006/2006_12_18_GSK945.htm.

[120] A. K. Ghosh, J. Li, H. Mitsuya, unpublished work, Purdue University and National Cancer Institute.

[121] T. Cihlar, G. X. He, X. Liu, J. M. Chen, M. Hatada, S. Swaminathan, M. J. McDermott, Z. Y. Yang, et al., *J. Mol. Biol.* **2006**, *363*, 635–647.

[122] C. Callebaut, K. Stray, L. Tsai, L. H. Xu, G. X. He, A. Mulato, T. Priskich, N. Parkin, et al., *20th International Conference on Antiviral Research*; Palm Spring, CA, April 29 to May 3, **2007**, p. 2.

[123] C. Callebaut, K. Stray, L. Tsai, M. Williams, Z. Yang, C. Cannizzaro, S. A. Leavitt, X. Liu, K. Wang, B. P. Murray, A. Mulato, M. Hatada, T. Priskich, N. Parkin, S. Swaminathan, W. Lee, G. He, L. Xu, T. Cihlar, *Antimicrob. Agents Chemother.* **2011**, *55*, 1366–1376.

[124] A. Gustchina, I. T. Weber, *FEBS Lett.* **1990**, *269*, 269–272.

[125] A. K. Ghosh, C. D. Martyr, M. Steffey, Y.-F. Wang, J. Agniswamy, M. Amano, I. T. Weber, H. Mitsuya, *ACS Med. Chem. Lett.* **2011**, *2*, 298–302.

[126] D. J. Kempf, K. C. Marsh, D. A. Paul, M. F. Knige, D. W. Norbeck, W. E. Kohlbrenner, L. Codacovi, S. Vasavanonda, P. Bryant, X. C. Wang, N. E. Wideburg, J. J. Clement, J. J. Plattner, J. Erickson, *Antimicrob. Agents Chemother.* **1991**, *35*, 2209–2214.

[127] E. T. Baldwin, T. N. Bhat, B. Liu, N. Pattabriaman, J. W. Erickson, *Struct. Biol.* **1995**, *2*, 244–249.

[128] Y. Tojo, Y. Koh, M. Amano, M. Aoki, D. Das, A. K. Ghosh, H. Mitsuya, *Antimicrob. Agents Chemother.* **2010**, *54*, 3460–3470.

[129] A. K. Ghosh, S. Gemma, J. Takayama, A. Baldridge, S. Leshchenko-Yashchuk, H. B. Miller, Y.-F. Wang, A. Y. Kovalevsky, Y. Koh, I. T. Weber, H. Mitsuya, *Org. Biomol. Chem.* **2008**, *6*, 3703–3713.

[130] A. K. Ghosh, B. Chapsal, G. L. Parham, M. P. Steffey, J. Agniswamy, Y.-F. Wang, M. Amano, I. T. Weber, H. Mitsuya, *J. Med. Chem.* **2011**, *54*, 5890–5901.

[131] A. K. Ghosh, S. Leshchenko-Yashchuk, D. D. Anderson, A. Baldridge, M. Noetzel, H. B. Miller, Y. Tie, Y.-F. Wang, Y. Koh, I. T. Weber, H. Mitsuya, *J. Med. Chem.* **2009**, *52*, 3902–3914.

[132] Y. Koh, D. Das, S. Leshchenko, H. Nakata, H. Ogata-Aoki, M. Amano, M. Nakayama, A. K. Ghosh, H. Mitsuya, *Antimicrob. Agents Chemother.* **2009**, *53*, 997–1006.

[133] A. K. Ghosh, S. Gemma, A. Baldridge, Y. F. Wang, A. Y. Kovalevsky, Y. Koh, I. T. Weber, H. Mitsuya, *J. Med. Chem.* **2008**, *51*, 6021–6033.

[134] A. K. Ghosh, B. Chapsal, A. Baldridge, M. P. Steffey, D. E. Walters, Y. Koh, M. Amano, H. Mitsuya, *J. Med. Chem.* **2011**, *54*, 622–634.

[135] K. Ide, M. Aoki, M. Amano, Y. Koh, R. S. Yedidi, D. Das, S. Leschenko, B. Chapsal, A. K. Ghosh, H. Mitsuya, *Antimicrob. Agents Chemother.* **2011**, *55*, 1717–1727.

[136] T. A. Halgren, *J. Comput. Chem.* **1999**, *20*, 730–748.

[137] A. K. Ghosh, C. X. Xu, K. V. Rao, A. Baldridge, J. Agniswamy, Y. F. Wang, I. T. Weber, M. Aoki, S. G. P. Miguel, M. Amano, H. Mitsuya, *ChemMedChem* **2010**, *5*, 1850–1854.

AAC
Journals.ASM.org

Mechanism of Interaction of Human Mitochondrial DNA Polymerase γ with the Novel Nucleoside Reverse Transcriptase Inhibitor 4′-Ethynyl-2-Fluoro-2′-Deoxyadenosine Indicates a Low Potential for Host Toxicity

Christal D. Sohl,[a] Kamlendra Singh,[b] Rajesh Kasiviswanathan,[c] William C. Copeland,[c] Hiroaki Mitsuya,[d,e] Stefan G. Sarafianos,[b] and Karen S. Anderson[a]

Department of Pharmacology, Yale University School of Medicine, New Haven, Connecticut, USA[a]; Department of Molecular Microbiology and Immunology, University of Missouri School of Medicine, Columbia, Missouri, USA[b]; Laboratory of Molecular Genetics, National Institute of Environmental Health Sciences, National Institutes of Health, DHHS, Research Triangle Park, North Carolina, USA[c]; Departments of Infectious Diseases and Hematology, Kumamoto University Graduate School of Medical Sciences, Kumamoto, Japan[d]; and Experimental Retrovirology Section, HIV and AIDS Malignancy Branch, National Cancer Institute, National Institutes of Health, Bethesda, Maryland, USA[e]

The potent antiretroviral 4′-ethynyl-2-fluoro-2′-deoxyadenosine (EFdA) is a promising experimental agent for treating HIV infection. Pre-steady-state kinetics were used to characterize the interaction of EFdA-triphosphate (EFdA-TP) with human mitochondrial DNA polymerase γ (Pol γ) to assess the potential for toxicity. Pol γ incorporated EFdA-TP 4,300-fold less efficiently than dATP, with an excision rate similar to ddATP. This strongly indicates EFdA is a poor Pol γ substrate, suggesting minimal Pol γ-mediated toxicity, although this should be examined under clinical settings.

Nucleoside reverse transcriptase inhibitors (NRTIs) are a critical component of highly active antiretroviral therapy for treating HIV infection. All FDA-approved NRTIs are nucleoside analogs lacking a 3′-hydroxyl group, forcing DNA chain termination upon incorporation by viral reverse transcriptase (RT). A central source of toxicity stems from the interaction of NRTIs with human mitochondrial DNA polymerase γ (Pol γ), the only human polymerase capable of using these drugs as substrates (2, 16, 18, 20). Incorporation of NRTIs can result in chain termination during replication, causing mitochondrial DNA depletion that can manifest in patients as myopathies, lipodystrophies, lactic acidosis, or liver failure (2–4, 12).

Current NRTIs can be plagued with toxicity and RT resistance, so there is a critical need for new antivirals. A promising new NRTI is 4′-ethynyl-2-fluoro-2′-deoxyadenosine (EFdA) (Fig. 1A) (17). Its 50% effective concentration (EC_{50}) of 50 pM is one of the best reported for an NRTI, 440-fold better than zidovudine (AZT) and 66,000-fold better than tenofovir, and numerous NRTI-resistant strains of HIV also show sensitivity and even hypersensitivity to EFdA (13, 17, 24, 27). It is also effective *in vivo*, causing a significant decrease in viral load and low toxicity in a humanized HIV-infected mouse model (9).

Despite the 3′-hydroxyl group, EFdA acts as a chain terminator by preventing RT translocation (24). This is in contrast to KP-1212, another 3′-hydroxyl-containing NRTI that facilitates error-prone extension by RT (1, 25). The 4′-ethynyl group locks the sugar in a favorable position for incorporation, which, along with the 3′-hydroxyl, makes EFdA a better substrate for RT than native nucleotides (15, 24). Similarly, EFdA may be preferred by Pol γ, but kinetic studies are limited to a 50% inhibitory concentration (IC_{50}) of 10 μM and a K_i of 25 μM for Pol γ (26, 27), indicating that EFdA serves as a substrate. In this study, we sought to expand our prior work with EFdA (26) to characterize the molecular mechanism of inhibition of Pol γ by EFdA. Such studies are critical to assess the safety of drugs in preclinical and clinical trials.

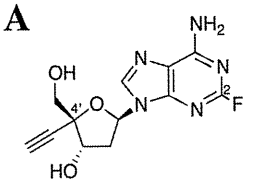

FIG 1 (A) Structure of EFdA. (B) DNA oligonucleotides used in the experiments. Shown are the D21 primer (radiolabeled, as indicated by an asterisk) and the D36 template. The primer "X" is the site of incorporation of the incoming dATP or EFdA-TP used in the single-nucleotide incorporation experiments or the location of the EFdA-MP to be removed in the excision studies.

Assessing the potential for Pol γ-mediated toxicity requires discerning the individual rate constants of NRTI incorporation and excision using pre-steady-state kinetics. Since steady-state studies report only on the rate-limiting step, which for Pol γ is product release, pre-steady-state kinetics are required to determine NRTI affinity and rates of NRTI incorporation and excision by Pol γ, which provides a detailed kinetic mechanism of *in vitro* toxicity. Single-turnover conditions, in which the enzyme is in excess of the substrate, were used to generate k_{pol}, the maximum rate of polymerization, and K_d, the binding affinity for the incom-

Received 14 September 2011 Returned for modification 7 November 2011
Accepted 2 December 2011
Published ahead of print 12 December 2011
Address correspondence to Karen S. Anderson, karen.anderson@yale.edu.

doi:10.1128/AAC.05729-11

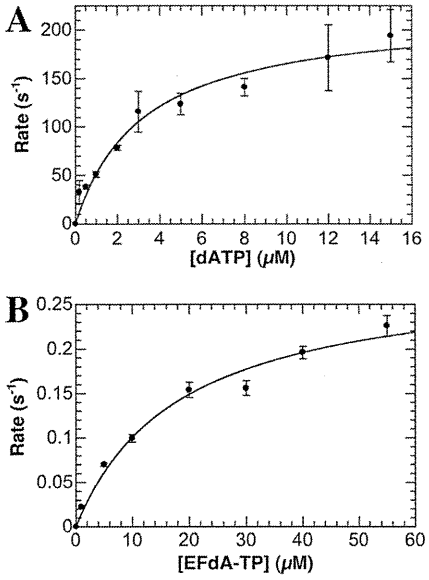

FIG 2 Concentration dependence of the observed rate of nucleotide incorporation by Pol γ. Each point in the plots represents the observed rate generated from fitting a time course with 10 different points using a double exponential equation (dATP) or a single exponential equation (EFdA-TP) (KaleidaGraph). The error bars in the plots represent the deviance from these exponential fits, and the standard errors associated with the determined rate constant values represent the deviance from the hyperbolic fits shown. (A) Observed rates of incorporation were plotted against dATP concentration and fit with a hyperbolic equation to generate a k_{pol} value of 220 ± 16 s^{-1} and a K_d value of 3.2 ± 0.7 μM. (B) Observed rates of incorporation were plotted against EFdA-TP concentration and fit with a hyperbolic equation to generate a k_{pol} value of 0.29 ± 0.02 s^{-1} and a K_d value of 18 ± 4 μM.

ing nucleotide, as described previously (7, 11). Wild-type (WT) Pol γ (exonuclease deficient) catalytic subunit (Pol γA) and accessory subunit were purified and reconstituted as described elsewhere (22, 23, 29). A KinTek Instruments RQF-3 rapid chemical quench was used to mix Pol γ holoenzyme and substrate, a 5′-radiolabeled DNA primer annealed to a DNA template (D21/D36 substrate) (Fig. 1B), with magnesium chloride and various concentrations of dATP or EFdA-triphosphate (EFdA-TP). The reaction was quenched with EDTA, and reaction mixtures were separated on a 20% polyacrylamide denaturing gel and analyzed by phosphorimaging (Bio-Rad Molecular Imager FX). Plots of product formation versus time were fit to single-exponential (EFdA-TP) or double-exponential (dATP) equations to generate k_{obs} (observed rate) values, which were plotted against nucleotide concentration and fit to a hyperbola to generate k_{pol} and K_d (KaleidaGraph; Synergy) (Fig. 2).

Pol γ incorporated EFdA-TP 760-fold more slowly and with 5.6-fold-lower affinity than the natural dATP substrate (Table 1). The efficiency of EFdA-TP incorporation (0.016 $\mu M^{-1} s^{-1}$) is well within the range of NRTIs on the market, showing 340- and 1.5-fold improvement over stavudine and didanosine, respectively (11). Although lower efficiencies are seen with tenofovir (3.2-fold) and AZT (16-fold) (11), it is important to remember that EFdA in the steady state showed 440-fold- and 66,000-fold-higher potency than AZT and tenofovir, respectively (24). Importantly, in contrast to RT, which shows a 2-fold selectivity for EFdA-TP over dATP in steady-state studies (24), Pol γ shows a 4,300-fold preference for the natural dATP substrate over EFdA-TP (Table 1), and this coupled

TABLE 1 Pre-steady-state rate constants for dNTP incorporation by Pol γ[a]

Nucleotide	k_{pol} (s^{-1})	K_d (μM)	Efficiency ($\mu M^{-1} s^{-1}$)[b]	Discrimination[c]
dATP	220 ± 16	3.2 ± 0.7	69	
EFdA-TP	0.29 ± 0.02	18 ± 4	0.016	4,300

[a] At least 7 different time courses containing 10 time points each were used to generate k_{pol} and K_d. The standard error estimates shown were derived from the deviance from the nonlinear regression fits determined using KaleidaGraph software.
[b] Efficiency = k_{pol}/K_d.
[c] Discrimination = efficiency$_{(dATP)}$/efficiency$_{(EFdA-TP)}$.

with the very low incorporation rate and low affinity for EFdA indicates a very low risk of Pol γ-mediated toxicity.

This rare EFdA incorporation event can be further mitigated via excision by Pol γ. To measure the rate of excision (k_{exo}), WT HIV-1 RT (purified as described previously [6, 14]) incorporated a single EFdA-TP into a D21/D36 substrate (Fig. 1B) (11). Under single-turnover conditions, exonuclease-competent Pol γ holoenzyme (purification detailed elsewhere [23]) and the D21-EFdA/D36 substrate were manually mixed with magnesium chloride, followed by quenching and product separation (Fig. 3A) (28). A plot of the percent loss of substrate versus time was fit to a

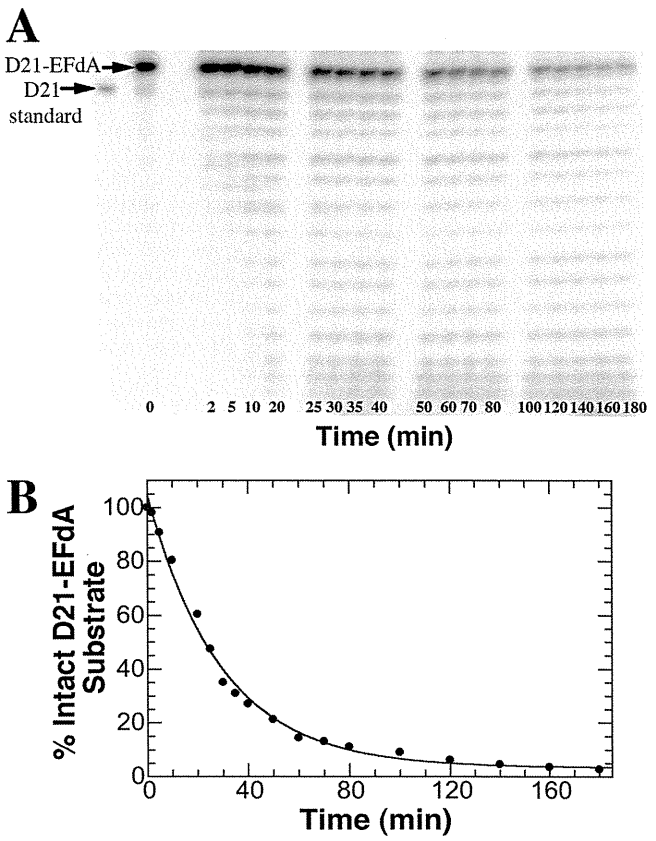

FIG 3 Excision of EFdA by Pol γ. (A) Gel analysis of the intact D21-EFdA substrate and degradation products over a 3-h time course. (B) A single exponential fitting of a plot of the percent loss of substrate versus time yielded a k_{exo} value of 0.00057 ± 0.00003 s^{-1}. Each point represents a single experiment within the time course, and the standard error associated with the k_{exo} value represents the deviance from this single exponential fitting as calculated by the KaleidaGraph software.

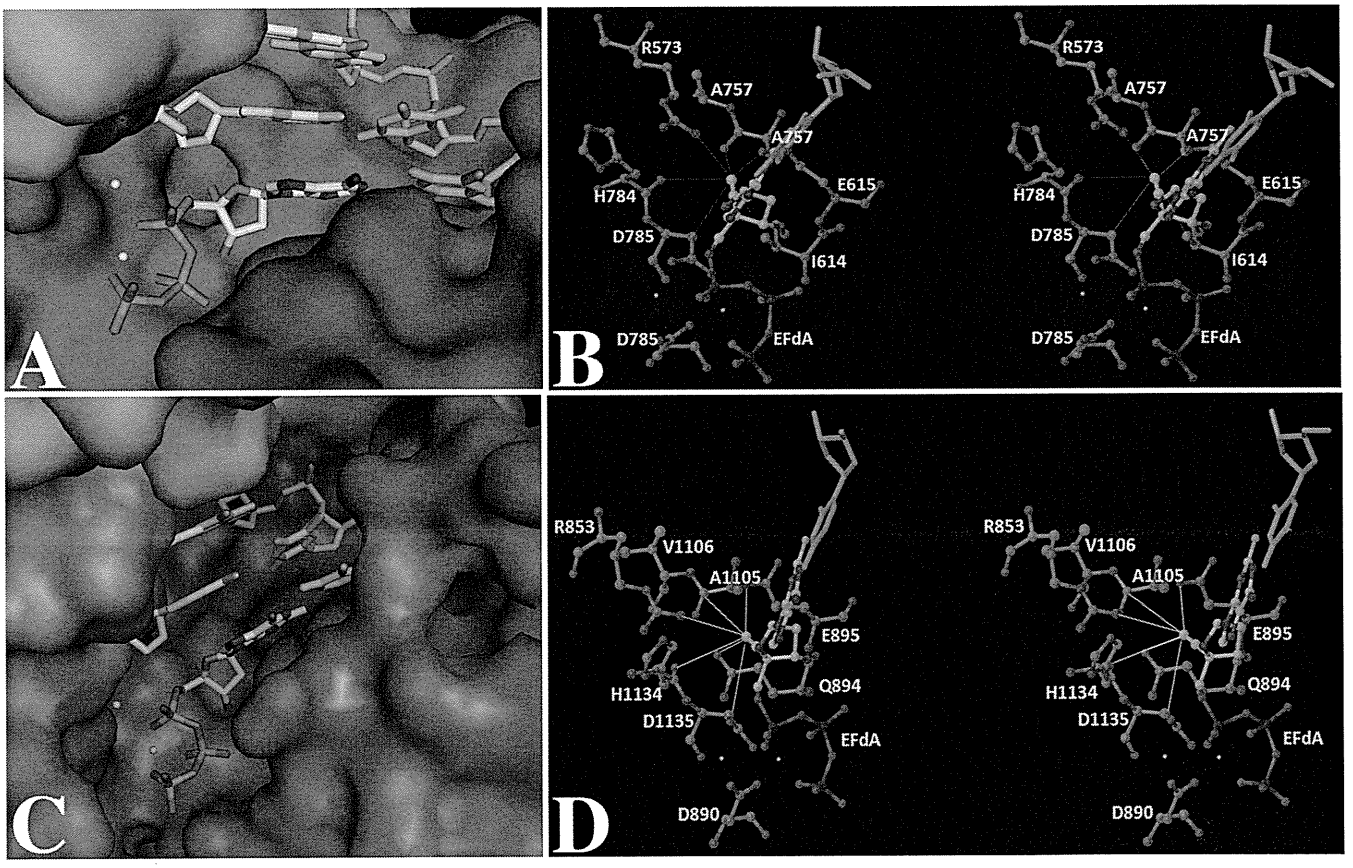

FIG 4 (A) KlenTaq–DNA–EFdA-TP. (B) KlenTaq–DNA–EFdA-TP in stereo view, highlighting interactions of the 4′-ethynyl group of EFdA-TP with the neighboring amino acid residues. (C) Pol γA–DNA–EFdA-TP. (D) Pol γA–DNA–EFdA-TP in stereo view, highlighting the interactions of 4′-ethynyl group of EfdA-TP with proximal amino acid residues. For (A) and (C), the ternary complex model of the polymerase subunit with template (cyan), primer (yellow), and EFdA-TP (colored by atom type as follows: carbon, gray; nitrogen, blue; oxygen, purple; phosphorous, orange). The enzyme is rendered as a Connolly surface representation with the thumb, palm, finger, and exonuclease domains colored in green, red, blue, and orange, respectively. For clear visualization of EFdA-TP, some residues at the tip of the fingers and thumb have been removed. However, these side chains were part of the computations. The metal ions are depicted as white spheres. For panels B and D, the amino acid residues (colored by atom type as follows: carbon, green; nitrogen, blue; oxygen, red) important for interaction with EFdA-TP (using the same color scheme, except carbon is colored gray and phosphorous purple) are highlighted. The template is shown in cyan. The thin lines depict the possible interactions with the amino acid residues in the vicinity of the 4′-ethynyl group of EFdA-TP. These interactions are not necessarily the hydrogen bonds. Interaction lengths range from 2.9 to 4 Å. Panels A and C were generated by PyMOL (http://www.pymol.org/), and panels B and D were generated by Maestro 9.1 (Schrödinger Inc., NY).

single exponential equation to generate k_{exo} (Fig. 3B). EFdA was excised at 0.00057 ± 0.00003 s^{-1}, yielding a half-life of ~20 min, similar to ddAMP removal (0.0005 s^{-1}) (11). Since DNA dissociates from Pol γ at 0.02 s^{-1} (10), it is likely that dissociation will occur before EFdA excision. The k_{exo} for EFdA falls in range of currently available NRTIs, 1.4-fold higher than for d4T and AZT (10) and much higher than for zalcitabine, which is too low to be detected (<0.00002 s^{-1}) (7), but 1.3-fold and 26-fold lower than for tenofovir (10) and lamivudine (7), respectively. Since dosages of EFdA are expected to be low due to the observed high potency, and because the Pol γ incorporation rate is very low with moderate EFdA excision rates, it is predicted that Pol γ-related toxicity will be limited. However, mitochondrial toxicity must be tested under clinical settings.

To probe the mechanism of the 4,300-fold increased efficiency of dATP incorporation over EFdA-TP, we used structural modeling to compare the dATP and EFdA-TP ternary complexes using the currently available Pol γ crystal structure (19). The active site residues of Pol γA are seen at topologically equivalent positions in other A family polymerases, including the large fragment of Pol I from *Thermus aquaticus* (KlenTaq), which has been reported with all four incoming ddNTPs (21). After superimposing Pol γA and KlenTaq using their active sites as a reference point, we docked 6 bp of DNA from the 3′ end of the primer, the ddATP, and two catalytic metal ions from the KlenTaq structure (PDB ID 1QSY [21]) into the Pol γ structure using Glide (Schrödinger Suite). Significant steric interactions involving residues M1057 to A1064, a region not found in other A family DNA polymerases (19), prevented energetically favorable docking of the template primer and ddATP at the Pol γA active site, and we deleted these residues because they are expected to undergo significant conformational changes in the ternary complex. Interestingly, similar changes are observed in N4 virion RNA polymerase, which undergoes a conformational change to displace a structurally equivalent region in order to accommodate duplex DNA (8).

The modeled KlenTaq–DNA–EFdA-TP ternary complex is shown in Fig. 4A and B for comparison with the Pol γA–DNA–EFdA-TP complex shown in Fig. 4C and D. The 4′-ethynyl group

of EFdA-TP is reasonably accommodated in a pocket defined by KlenTaq residues I614, E615, R753, and H784 (corresponding to Q894, E895, R853, and H1134 in Pol γ), which are 4.2, 3.5, 3.3, and 4.6 Å, respectively, away from this group, consistent with a relatively small change in affinity for EFdA-TP versus dATP (Table 1). A measureable K_i value (25 μM) has been determined for EFdA-TP (26), supporting the hypothesis that the binding pocket is similar for EFdA-TP and dATP. To probe this idea further, we employed a pre-steady-state competition assay in which the rate of dATP incorporation by the Pol γ holoenzyme was measured in the presence of various concentrations of EFdA-TP. EFdA-TP was able to compete with dATP for the binding pocket, as indicated by a linear decrease in the k_{obs}, although concentrations higher than the K_d for EFdA binding (18 μM) were required to lower the rate of incorporation of 3 μM dATP (the K_d of dATP) (data not shown). To achieve a 4.8-fold drop in the rate of dATP incorporation, a concentration of EFdA-TP at nearly 6 times its K_d was required (data not shown). Overall, this competition experiment supports our model of a similar binding pocket for EFdA-TP and dATP, leading to only minor changes in K_d, as well as our finding that EFdA-TP is a poor competitor of dATP due to its inefficient incorporation.

The 4′-ethynyl group of EFdA appears to be in the proximity of E895 in Pol γ (E615 in KlenTaq) and may disturb hydrogen bonding with Y955 (Y671 in KlenTaq), which is required for efficient catalysis in the Pol I family (Fig. 4). This may explain the severe defects in k_{pol} observed for EFdA incorporation. Interestingly, incorporation of 4′-alkyl-modified nucleoside analogs by the Klenow fragment of DNA Pol I from *Escherichia coli* showed a lower k_{pol} (~60-fold), with a small loss of affinity (~1.5-fold), similar to that for EFdA (5).

In summary, we have investigated the effects of a novel NRTI, EFdA, on Pol γ. EFdA has shown great promise in preclinical trials for the treatment of HIV infection because of its high potency and low toxicity. We show that this low toxicity is due in part to extremely inefficient EFdA incorporation and, to a lesser extent, subsequent EFdA excision by human Pol γ. Structural modeling suggests that the relatively small change in affinity for EFdA-TP relative to dATP is due to similar accommodation within a pocket, while the severe decrease in k_{pol} may be due to hydrogen bond disruption by EFdA. Characterizing the ability of Pol γ to incorporate NRTIs into a DNA template is critical to assess the safety of new drugs in this important class of antivirals.

ACKNOWLEDGMENTS

This work was supported by NIH grants R01 GM049551 (to K.S.A.), F32 GM099289 (to C.D.S.), AI094715, AI076119, AI079801, and AI074389 (to S.G.S.) and by the Intramural Research Program of the NIH, NIEHS, ES 065080 (to W.C.C.).

Additionally, C.D.S. and K.S.A. thank Ligong Wang and Krasimir Spasov for the purification of the Pol γ accessory subunit and RT, respectively.

REFERENCES

1. **Anderson JP, Daifuku R, Loeb LA.** 2004. Viral error catastrophe by mutagenic nucleosides. Annu. Rev. Microbiol. **58**:183–205.
2. **Brinkman K, Kakuda TN.** 2000. Mitochondrial toxicity of nucleoside analogue reverse transcriptase inhibitors: a looming obstacle for long-term antiretroviral therapy? Curr. Opin. Infect. Dis. **13**:5–11.
3. **Brinkman K, Smeitink JA, Romijn JA, Reiss P.** 1999. Mitochondrial toxicity induced by nucleoside-analogue reverse-transcriptase inhibitors is a key factor in the pathogenesis of antiretroviral-therapy-related lipodystrophy. Lancet **354**:1112–1115.
4. **Dalakas MC, et al.** 1990. Mitochondrial myopathy caused by long-term zidovudine therapy. N. Engl. J. Med. **322**:1098–1105.
5. **Di Pasquale F, et al.** 2008. Opposed steric constraints in human DNA polymerase beta and *E. coli* DNA polymerase I. J. Am. Chem. Soc. **130**: 10748–10757.
6. **Feng JY, Anderson KS.** 1999. Mechanistic studies comparing the incorporation of (+) and (-) isomers of 3TCTP by HIV-1 reverse transcriptase. Biochemistry **38**:55–63.
7. **Feng JY, Johnson AA, Johnson KA, Anderson KS.** 2001. Insights into the molecular mechanism of mitochondrial toxicity by AIDS drugs. J. Biol. Chem. **276**:23832–23837.
8. **Gleghorn ML, Davydova EK, Rothman-Denes LB, Murakami KS.** 2008. Structural basis for DNA-hairpin promoter recognition by the bacteriophage N4 virion RNA polymerase. Mol. Cell **32**:707–717.
9. **Hattori S, et al.** 2009. Potent activity of a nucleoside reverse transcriptase inhibitor, 4′-ethynyl-2-fluoro-2′-deoxyadenosine, against human immunodeficiency virus type 1 infection in a model using human peripheral blood mononuclear cell-transplanted NOD/SCID Janus kinase 3 knockout mice. Antimicrob. Agents Chemother. **53**:3887–3893.
10. **Johnson AA, Johnson KA.** 2001. Exonuclease proofreading by human mitochondrial DNA polymerase. J. Biol. Chem. **276**:38097–38107.
11. **Johnson AA, et al.** 2001. Toxicity of antiviral nucleoside analogs and the human mitochondrial DNA polymerase. J. Biol. Chem. **276**:40847–40857.
12. **Kakuda TN, Brundage RC, Anderson PL, Fletcher CV.** 1999. Nucleoside reverse transcriptase inhibitor-induced mitochondrial toxicity as an etiology for lipodystrophy. AIDS **13**:2311–2312.
13. **Kawamoto A, et al.** 2008. 2′-Deoxy-4′-*C*-ethynyl-2-halo-adenosines active against drug-resistant human immunodeficiency virus type 1 variants. Int. J. Biochem. Cell Biol. **40**:2410–2420.
14. **Kerr SG, Anderson KS.** 1997. RNA dependent DNA replication fidelity of HIV-1 reverse transcriptase: evidence of discrimination between DNA and RNA substrates. Biochemistry **36**:14056–14063.
15. **Kirby KA, et al.** 2011. The sugar ring conformation of 4′-ethynyl-2-fluoro-2′-deoxyadenosine and its recognition by the polymerase active site of HIV reverse transcriptase. Cell. Mol. Biol. (Noisy-le-grand) **57**:40–46.
16. **Koczor CA, Lewis W.** 2010. Nucleoside reverse transcriptase inhibitor toxicity and mitochondrial DNA. Expert Opin. Drug Metab. Toxicol. **6**:1493–1504.
17. **Kodama EI, et al.** 2001. 4′-Ethynyl nucleoside analogs: potent inhibitors of multidrug-resistant human immunodeficiency virus variants *in vitro*. Antimicrob. Agents Chemother. **45**:1539–1546.
18. **Kohler JJ, Lewis W.** 2007. A brief overview of mechanisms of mitochondrial toxicity from NRTIs. Environ. Mol. Mutagen. **48**:166–172.
19. **Lee YS, Kennedy WD, Yin YW.** 2009. Structural insight into processive human mitochondrial DNA synthesis and disease-related polymerase mutations. Cell **139**:312–324.
20. **Lewis W, Day BJ, Copeland WC.** 2003. Mitochondrial toxicity of NRTI antiviral drugs: an integrated cellular perspective. Nat. Rev. Drug Discov. **2**:812–822.
21. **Li Y, Kong Y, Korolev S, Waksman G.** 1998. Crystal structures of the Klenow fragment of *Thermus aquaticus* DNA polymerase I complexed with deoxyribonucleoside triphosphates. Protein Sci. **7**:1116–1123.
22. **Lim SE, Longley MJ, Copeland WC.** 1999. The mitochondrial p55 accessory subunit of human DNA polymerase gamma enhances DNA binding, promotes processive DNA synthesis, and confers *N*-ethylmaleimide resistance. J. Biol. Chem. **274**:38197–38203.
23. **Longley MJ, Ropp PA, Lim SE, Copeland WC.** 1998. Characterization of the native and recombinant catalytic subunit of human DNA polymerase gamma: identification of residues critical for exonuclease activity and dideoxynucleotide sensitivity. Biochemistry **37**:10529–10539.
24. **Michailidis E, et al.** 2009. Mechanism of inhibition of HIV-1 reverse transcriptase by 4′-ethynyl-2-fluoro-2′-deoxyadenosine triphosphate, a translocation-defective reverse transcriptase inhibitor. J. Biol. Chem. **284**: 35681–35691.
25. **Murakami E, Basavapathruni A, Bradley WD, Anderson KS.** 2005. Mechanism of action of a novel viral mutagenic covert nucleotide: molecular interactions with HIV-1 reverse transcriptase and host cell DNA polymerases. Antiviral Res. **67**:10–17.
26. **Nakata H, et al.** 2007. Activity against human immunodeficiency virus type 1, intracellular metabolism, and effects on human DNA polymerases

of 4′-ethynyl-2-fluoro-2′-deoxyadenosine. Antimicrob. Agents Chemother. 51:2701–2708.
27. **Ohrui H, et al.** 2007. 2′-Deoxy-4′-*C*-ethynyl-2-fluoroadenosine: a nucleoside reverse transcriptase inhibitor with highly potent activity against wide spectrum of HIV-1 strains, favorable toxic profiles, and stability in plasma. Nucleosides Nucleotides Nucleic Acids **26**:1543–1546.
28. **Ray AS, et al.** 2007. Interaction of 2′-deoxyguanosine triphosphate analogue inhibitors of HIV reverse transcriptase with human mitochondrial DNA polymerase gamma. Antivir. Chem. Chemother. **18**:25–33.
29. **Yakubovskaya E, Chen Z, Carrodeguas JA, Kisker C, Bogenhagen DF.** 2006. Functional human mitochondrial DNA polymerase gamma forms a heterotrimer. J. Biol. Chem. **281**:374–382.

Published online 8 September 2011

Nucleic Acids Research, 2012, Vol. 40, No. 1 ***345–359***
doi:10.1093/nar/gkr694

Biochemical, inhibition and inhibitor resistance studies of xenotropic murine leukemia virus-related virus reverse transcriptase

Tanyaradzwa P. Ndongwe[1], Adeyemi O. Adedeji[1], Eleftherios Michailidis[1], Yee Tsuey Ong[1], Atsuko Hachiya[1], Bruno Marchand[1], Emily M. Ryan[1], Devendra K. Rai[1], Karen A. Kirby[1], Angela S. Whatley[1], Donald H. Burke[1,2], Marc Johnson[1], Shilei Ding[3], Yi-Min Zheng[1], Shan-Lu Liu[1,3], Ei-Ichi Kodama[4], Krista A. Delviks-Frankenberry[5], Vinay K. Pathak[5], Hiroaki Mitsuya[6], Michael A. Parniak[7], Kamalendra Singh[1] and Stefan G. Sarafianos[1,2,*]

[1]Christopher Bond Life Sciences Center, Department of Molecular Microbiology & Immunology, University of Missouri, School of Medicine, Columbia, [2]Department of Biochemistry, University of Missouri, Columbia, MO 65211, USA, [3]Department of Microbiology and Immunology, McGill University, Montreal, QC, Canada, [4]Department of Internal Medicine, Division of Emerging Infectious Diseases, Tohoku University School of Medicine, Sendai, Japan, [5]HIV Drug Resistance Program, National Cancer Institute-Frederick, Frederick MD, [6]Department of Internal Medicine, Kumamoto University School of Medicine, Kumamoto Japan & Experimental Retrovirology Section, HIV/AIDS Malignancy Branch, NIH, Bethesda MD and [7]Department of Molecular Genetics & Biochemistry, University of Pittsburgh School of Medicine, Pittsburgh, PA, USA

Received June 3, 2011; Revised August 5, 2011; Accepted August 8, 2011

ABSTRACT

We report key mechanistic differences between the reverse transcriptases (RT) of human immunodeficiency virus type-1 (HIV-1) and of xenotropic murine leukemia virus-related virus (XMRV), a gammaretrovirus that can infect human cells. Steady and pre-steady state kinetics demonstrated that XMRV RT is significantly less efficient in DNA synthesis and in unblocking chain-terminated primers. Surface plasmon resonance experiments showed that the gammaretroviral enzyme has a remarkably higher dissociation rate (k_{off}) from DNA, which also results in lower processivity than HIV-1 RT. Transient kinetics of mismatch incorporation revealed that XMRV RT has higher fidelity than HIV-1 RT. We identified RNA aptamers that potently inhibit XMRV, but not HIV-1 RT. XMRV RT is highly susceptible to some nucleoside RT inhibitors, including Translocation Deficient RT inhibitors, but not to non-nucleoside RT inhibitors. We demonstrated that XMRV RT mutants K103R and Q190M, which are equivalent to HIV-1 mutants that are resistant to tenofovir (K65R) and AZT (Q151M), are also resistant to the respective drugs, suggesting that XMRV can acquire resistance to these compounds through the decreased incorporation mechanism reported in HIV-1.

INTRODUCTION

Xenotropic murine leukemia virus-related virus (XMRV) is a gammaretrovirus that was first identified in some prostate cancer tissues (1,2) While some subsequent reports confirmed the presence of XMRV in prostate cancer samples (3–6), several others found little or no evidence of the virus in patient samples (7–9). XMRV DNA was also reported in 67% of patients with chronic fatigue syndrome (CFS) (10), but several subsequent studies in Europe and the USA failed to identify XMRV DNA in CFS patients or healthy controls (11–15). Hence, the relevance of XMRV to human disease remains unclear (16) and have been challenged (17). Most recently, it has been reported that XMRV has been generated through recombination of two separate proviruses suggesting that the association of XMRV with human disease is due to contamination of human samples with virus originating from this recombination event (18). Nonetheless, as a retrovirus that can infect human cells, XMRV can be very helpful in advancing our understanding of the mechanisms of retroviral reverse transcription, inhibition and drug resistance.

*To whom correspondence should be addressed. Tel: +1 573 882 4338; Fax: +1 573 884 9676; Email: sarafianoss@missouri.edu

XMRV RT is similar to the Moloney murine leukemia virus (MoMLV) RT, which has been the subject of structural and biochemical studies (19–24). Most of the differences between these gammaretroviral enzymes are at the RNase H domain (Supplementary Figure S1). Comparisons of human immunodeficiency virus type-1 (HIV) RT with MoMLV RT have revealed structural and sequence differences (21). For example, HIV-1 RT is a heterodimer composed of two related subunits (25,26) [reviewed in (27,28)]. Its larger p66 subunit (~66 kDa) contains both the polymerase and RNase H domains; the smaller p51 subunit, (~51 kDa), is derived from the p66 subunit by proteolytic cleavage and its role is to provide structural support and optimize RT's biochemical functions (29). In contrast, structural studies have demonstrated that MoMLV RT is a monomer of about 74 kDa, although one study reported that it may form a homodimer during DNA synthesis (30). So far, there are no published biochemical or structural studies on XMRV RT. Hence, the present study on this enzyme and its comparison to related enzymes provides an excellent opportunity to advance our biochemical understanding of the mechanism of reverse transcription, its inhibition and drug resistance.

MATERIALS AND METHODS

Expression and purification of XMRV, HIV-1 and MoMLV RTs

The plasmid pBSK-XMRV containing the coding sequence of XMRV RT from the VP62 clone (GenBank: DQ399707.1) was chemically synthesized and optimized for bacterial expression by Epoch Biolabs Inc (Missouri City, Texas, USA). The 2013 bp XMRV RT sequence was amplified from pBSK-XMRVRT by PCR, using the forward and reverse primers 1 (all primer sequences are shown in Supplementary Table S1), resulting in NdeI and HindIII restriction sites. Drug resistant XMRV RT mutants Q190M and K103R (equivalent to HIV-1 Q151M RT and K65R) were generated by site-directed mutagenesis using forward and reverse primers 2 and 3. The digested amplicons were ligated into pET-28a (Novagen), resulting into a construct that expresses an N-terminal hexahistidine tag. pET-28a-MRT encoding full-length wild-type MoMLV RT was provided by Dr M. Modak (New Jersey Medical School, Newark NJ, USA).

Expression and purification of MoMLV and XMRV RTs were carried out similarly to our previously published protocols (23,24). Briefly, RTs were expressed in BL21-pLysS *Escherichia coli* (Invitrogen) grown at 37°C and induced with 150 μM IPTG at OD_{600} 0.8, followed by 16 h growth at 17°C. A cell pellet from a 3 l culture was incubated with 40 ml lysis buffer (50 mM Tris–HCl, pH 7.8, 500 mM NaCl, 1 mM PMSF, 0.1% NP-40, 1% sucrose and 2 mg/ml lysozyme), then sonicated and centrifuged at 15,000 *g* for 30 min. The supernatant was diluted 2-fold in Buffer A (50 mM Tri–HCl pH 7.8, 1 mM PMSF, 4% streptomycin sulfate and 10% sucrose), stirred on ice for 30 min and centrifuged. The supernatant was loaded on a Ni-NTA column and bound proteins were washed with 20 ml Buffer B (20 mM Tris–HCl pH 7.5, 500 mM NaCl) and 5 mM imidazole, followed by 20 ml Buffer B with 75 mM imidazole. RT was eluted in 2 ml fractions with 20 ml buffer B containing 300 mM imidazole. Fractions with RT were pooled and further purified by size exclusion chromatography (Superdex 75; GE Healthcare). RTs (>95% pure) were stored in 50 mM Tris–HCl pH 7.0, 100 mM NaCl, 1 mM DTT, 0.1% NP-40 and 30% glycerol in 10 μl aliquots at −20°C. Protein concentrations were determined by measuring UV_{280} (molar extinction coefficients of 106 and 103 $M^{-1}cm^{-1}$ for XMRV and MoMLV RT).

HIV-1 RT was cloned in a pETduo vector and purified as described previously (29,31,32). Oligonucleotide sequences (IDT-Coralville, IA, USA) of DNA/RNA substrates are shown in Supplementary Table S1. Nucleotides were purchased from Fermentas (Glen Burnie, MD, USA). They were treated with inorganic pyrophosphatase (Roche Diagnostics, Mannheim, Germany) as described previously (33) to remove PPi that might interfere with excision assays.

Steady state kinetics

Steady state parameters K_m and k_{cat} for dATP incorporation were determined using single nucleotide incorporation gel-based assays. XMRV RT and MoMLV RT reactions were carried out in 50 mM Tris–HCl pH 7.8, 60 mM KCl, 0.1 mM DTT, 0.01% NP-40 and 0.01% bovine serum albumin (BSA) (Reaction Buffer) with 6 mM $MgCl_2$ or 1.5 mM $MnCl_2$, 0.5 mM EDTA, 200 nM or 100 nM T_{d26}/5′-Cy3-P_{d18b}, 20 nM or 5 nM RT for XMRV and MoMLV RTs, respectively and varying concentrations of dNTP in a final volume of 10 μl. The reactions for HIV-1 RT were carried out in Reaction Buffer with 100 nM T_{d26}/5′-Cy3-P_{d18b}, 10 nM HIV-1 RT and 6 mM $MgCl_2$ in a 20 μl reaction. All the concentrations mentioned here and in subsequent assays reflect final concentration of reactants otherwise mentioned reactions were stopped after 15 min for XMRV, 4 min for MoMLV RT, and 2.5 min for HIV-1. The products were resolved on 15% polyacrylamide–7M urea gels. The gels were scanned with a Fuji Fla-5000 PhosphorImager (Stamford, CT, USA) and the bands were quantified using MultiGauge. Results were plotted using GraphPad Prism 4. K_m and k_{cat} were determined graphically using Michaelis–Menten equation.

Gel mobility shift assays

Formation of RT-DNA binary complex: 20 nM T_{d31}/5′-Cy3-P_{d18a} (Supplementary Table S1) was incubated for 10 minutes with increasing amounts of MoMLV or XMRV RT in 50 mM Tris–HCl pH 7.8, 0.01% BSA, 5 mM $MgCl_2$ and 10% (v/v) sucrose. The complexes were resolved on native 6% polyacrylamide 50 mM Tris–borate gel and visualized as described above.

Active site titration and determination of $K_{D.DNA}$

Active site concentrations and kinetic constants of DNA binding for XMRV, HIV-1 and MoMLV RTs were determined using pre-steady state experiments. Reactions

with XMRV and MoMLV RTs were carried out in the reaction buffers listed above. For XMRV RT 100 nM protein was pre-incubated with increasing concentrations of T_{d31}/5′-Cy3-P_{d18a}, followed by rapid mixing with a reaction mixture containing 5 mM $MgCl_2$ and 100 μM next incoming nucleotide (dATP). The reactions were quenched at various times (5 ms to 4 s) by adding EDTA to a final concentration of 50 mM. The amounts of 19-mer product were quantified and plotted against time. The data were fit to the following burst equation:

$$P = A(1 - e^{-k_{obs}t}) + k_{ss}t \quad (1)$$

where A is the amplitude of the burst phase that represents the RT–DNA complex at the start of the reaction, k_{obs} is the observed burst rate constant for dNTP incorporation, k_{ss} is the steady state rate constant and t is the reaction time. The rate constant of the linear phase (k_{cat}) was estimated by dividing the slope of the linear phase by the enzyme concentration. The active site concentration and T/P binding affinity ($K_{D.DNA}$) were determined by plotting the amplitude (A) against the concentration of T/P. Data were fit to the quadratic equation (Equation 2) using non-linear regression:

$$A = 0.5(K_D + [RT] + [DNA] - \sqrt{0.25(K_D + [RT] + [DNA])^2} - ([RT] + [DNA])) \quad (2)$$

where K_D is the dissociation constant for the RT–DNA complex, and [RT] is the concentration of active polymerase. HIV-1 RT's DNA binding affinity was determined as previously described (29).

Surface plasmon resonance assay

We used surface plasmon resonance (SPR) to measure the binding constants of XMRV and HIV-1 RTs to double-stranded DNA. Experiments were carried out using a Biacore T100 (GE Healthcare). To prepare the sensor chip surface we used the 5′-biotin-T_{d37}/P_{d25} oligonucleotide (Supplementary Table S1). One hundred and twenty RUs of this DNA duplex were bound in channel 2 of a streptavidin-coated sensor chip [Series S Sensor Chip SA (certified)] by flowing a solution of 0.1 μM DNA at a flow rate of 10 μl/min in a buffer containing 50 mM Tris pH 7.8, 50 mM NaCl. The binding constants were determined as follows: RT binding was observed by flowing solutions containing increasing concentrations of the enzyme (0.2, 0.5, 1, 2, 5, 10, 20, 50, 100 and 200 nM) in 50 mM Tris pH 7.8, 60 mM KCl, 1 mM DTT, 0.01% NP40 and 10 mM $MgCl_2$ in channels 1 (background) and 2 (test sample) at 30 μl/min. The trace obtained in channel 1 was subtracted from the trace in channel 2 to obtain the binding signal of RT. This signal was analyzed using the Biacore T100 Evaluation software to determine $K_{D.DNA}$, k_{on} and k_{off}.

Pre-steady state kinetics of dNTP incorporation

The optimal nucleotide incorporation rates (k_{pol}) were obtained by pre-steady state kinetics analysis using single nucleotide incorporation assays. A solution containing XMRV RT (150 nM final concentration) and T_{d31}/5′-Cy3-P_{d18a} (40 nM) was rapidly mixed with a solution of $MgCl_2$ (5 mM) and varying dATP (5–200 μM) for 0.1 to 6 s before quenching with EDTA (50 mM) (all concentrations in parentheses are final, unless otherwise stated). Products were resolved and quantified as described above. Burst phase incorporation rates and substrate affinities were obtained from fitting the data to Equation 1. Turnover rates (k_{pol}), dNTP binding to the RT-DNA complex ($K_{d.dATP}$), and observed burst rates (k_{obs}) were fit to the hyperbolic equation:

$$k_{obs} = (k_{pol}[dNTP])/(K_{d.dNTP} + [dNTP]) \quad (3)$$

HIV-1 RT's DNA binding affinity was determined as previously described (29).

Fidelity of DNA synthesis

The fidelity (error-proneness) of XMRV RT was determined and compared with that of MoMLV RT and HIV-1 RT by primer extension assays using 10 nM heteropolymeric T_{d100}/5′-Cy3-P_{d18a}. Reactions (10 μl) were carried out in Reaction Buffer containing all four dNTPs (100 μM each) or only three dNTPs (missing either dATP, dGTP or dTTP) at 100 μM each. Incubations of the XMRV and MoMLV (50 nM) reactions were at 37°C for 45 min and 30 min for HIV-1 RT (20 nM). Reactions were initiated by adding dNTPs, stopped with equal volume of formamide-bromophenol blue, and an aliquot was run on a 16% polyacrylamide–7M urea gel.

Kinetics of mismatch incorporation

For these experiments, instead of including the next correct nucleotide (dATP) in the polymerase reactions, we used dTTP as the mismatched incoming nucleotide. Hence, 50 nM XMRV RT was pre-incubated with 35 nM T_{d31}/5′-Cy3-P_{d18a} in reaction mixture. Reactions were initiated by adding dTTP (5–750 μM) and 5 mM $MgCl_2$, followed by incubation (37°C) for 5 min, due to the decreased mismatch incorporation rate of XMRV. For MoMLV RT, 30 nM RT and 20 nM DNA used and the reactions were carried out for 2.5 minutes. For HIV-1, 30 nM RT, 20 nM DNA and 0–200 μM nucleotide were used and the reactions were carried out for 2.5 min. The amount of extended primer was quantified and plotted against the concentration of dTTP. The data were used to derive the $K_{d.dNTP}$ of incorrect nucleotide binding, the rate k_{pol} (using Equations 1 and 3) and the efficiency of the misincorporation reaction ($k_{pol}/K_{d.dTTP}$).

Determination of *in vivo* fidelity

ANGIE P cells, which contain a retroviral vector (GA-1) that encodes a bacterial β-galactosidase gene (*lacZ*) and a neomycin phosphotransferase gene, were plated (5×10^6 cells/100 mm dish) and after 24 h were transfected using the calcium phosphate precipitation method with a plasmid expressing either XMRV or amphotropic MLV (AM-MLV) (three independent transfections per vector). After 48 h, the culture medium with XMRV or (AM-MLV) was harvested, serially diluted and used to infect